Theory and Practice of Determining the Dynamic Performance of Traction Rolling Stock

Janat Musayev *, Algazy Zhauyt, Sarakul Ismagulov, Saltanat Yusupova

Posted Date: 7 September 2023

doi: 10.20944/preprints202309.0483.v1

Keywords: locomotive; railway track; wheelset; dynamic characteristics; dynamic coefficient; analysis.

Article

Theory and Practice of Determining the Dynamic Performance of Traction Rolling Stock

Janat Musayev [1,*], Algazy Zhauyt [2], Sarakul Ismagulov [1] and Saltanat Yusupova [2]

[1] Department of Rolling Stock, Academy of Logistics and Transport; mussayev75@yandex.kz (J.M.); i.sarakul@alt.edu.kz (S.I.)

[2] Department of Electronics and Robotics, Almaty University of Power Engineering and Telecommunications named after G. Daukeyev; ali84jauit@mail.ru (A.Z.); s.yusupova@aues.kz (S.Y.)

* Correspondence: mussayev75@yandex.kz; Tel.: +77773626276, +77477871975

Abstract: In the interaction of the rolling stock and the upper structure of the railway track, intense dynamic loads occur. They have a destructive effect both on the parts of the rolling stock and on the elements of the superstructure of the track. In order to develop a durable, rational and reliably functioning design of cars and locomotives with good dynamic properties and good indicators of the impact of rolling stock on the railway track, along with theoretical computational studies, experimental studies are also required, which are usually the final stage in the design and implementation of rolling stock or modernization of existing ones. Locomotives and wagons in order to improve their strength and dynamic performance. The article presents the results of field tests to determine the dynamic performance of the type CKD6e diesel locomotive. The description of the preparation of the CKD6e shunting locomotive for testing is given. An analysis of the dynamic performance of a diesel locomotive during the passage of turnouts, on a straight section of the track and in a curve with a radius of 400 m, was carried out. The studies performed showed that the minimum value of the stability factor against wheel derailment on a straight section of the track is significantly higher than the standard value. The experimentally obtained ratio of frame forces to the static load from the wheelset on the rails, the coefficients of vertical dynamics of the first and second stages of suspension and the coefficient of stability against derailment of the wheel from the rail, registered on the track section in a curve with a radius of 400 m) meet the current requirements. A calculation scheme and equations of vertical oscillations are proposed, an analysis is carried out according to the graphs of movements of bogies and a locomotive body when moving along irregularities of different lengths at different speeds.

Keywords: locomotive; railway track; wheelset; dynamic characteristics; dynamic coefficient; analysis

1. Introduction

Experimental studies and full-scale tests are also carried out with the aim of further developing the design theory, studying the behavior of rolling stock in operating conditions, especially at high speeds [1]. Experimental research is also necessary in the development of new theoretical methods for studying the strength and dynamics of locomotives and cars, as well as in refining existing theoretical methods for studying rolling stock [2]. Dynamic train (running) tests are one of the main stages of working out the design of a locomotive and assessing its dynamic and strength qualities. Depending on the goals, they are general dynamic and special [3]. General dynamic tests include:

- factory, carried out by the manufacturer [4]. Their purpose is to check the operation of individual units of the locomotive and its design as a whole; according to the results of these tests, the manufacturer refines the prototype locomotive [5];
- acceptance train tests, during which the compliance of the dynamic qualities of the locomotive with the requirements of the locomotive customers and all applicable standards for the calculation and operation of locomotives is checked [6]. During these tests, the driving characteristics of the locomotive are determined (running smoothness, stability against transverse overturning of the locomotive in curves, stability of the wheel on the rail), dynamic

 doi:10.20944/preprints202309.0483.v1

forces acting on the elements of the locomotive and the railway track, dynamic forces that determine the strength and reliability of the locomotive in long-term operation [7].

As a result of processing the experimental data of rolling stock tests, stable correlations were obtained between various indicators of the dynamics of the rolling stock, the state of the track and the indicators of the stressed state of the track. In the general case, in the interaction of the track and rolling stock, dynamic indicators are associated with a large number of factors [8].

2. Preparing the CKD6e shunting locomotive for testing

The preparation of the CKD6E shunting locomotive included the following steps:

- installation of load cells;
- installation of displacement sensors;
- installation of acceleration sensors [9].

The location of the sensors on the locomotive is shown in Figure 1.

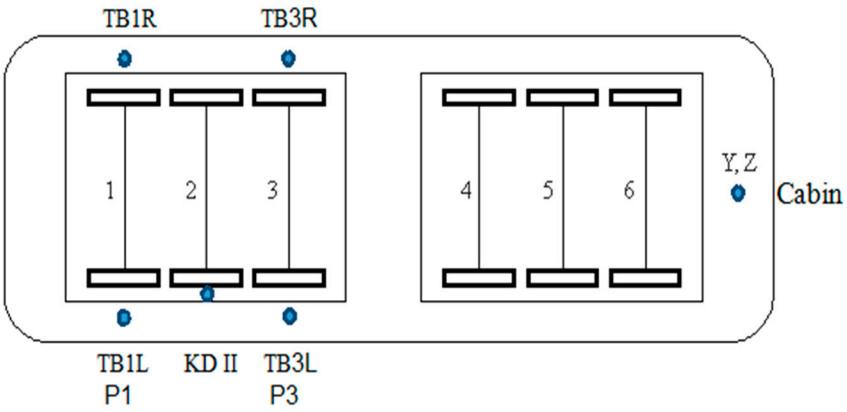

Figure 1. Placement of sensors for registration of processes to determine the dynamic performance of the type CKD6e-2108 diesel locomotive.

Figure 1 shows the following elements:

P1, P3 – frame forces of the 1st and 3rd wheelset (transverse movements between the bogie frame and the wheelset);

TB1L, TB1R, TB3L, TB3R - vertical movements between the bogie frame and the axle box of the 1st and 3rd wheelset on the left and right sides;

KD II - coefficient of vertical dynamics of the second stage of spring suspension (strain diagram);

Y, Z - accelerations on the floor in the cabin in the transverse and vertical directions.

Installation of load cells consists of 5 stages:

1 Marking the places of installation of sensors;
2 Cleaning the places where the sensors are installed;
3 Installation of sensors;
4 Assembly of circuits and verification;
5 Circuit isolation.

When marking the location of the installation of sensors on the bogie of the locomotive, the places most prone to deformation during the movement of the locomotive are taken into account. The locations of the sensors were chosen empirically [10]. The sensor installation sites are pre-cleaned with special equipment to a flat and smooth surface, and then the place is processed with sandpaper across the sensor installation to a slight roughness [11]. This work must be done at all marked places for installing sensors (see Figure 2).

Preprints (www.preprints.org) | NOT PEER-REVIEWED | Posted: 7 September 2023 doi:10.20944/preprints202309.0483.v1

Installation of sensors consists of the following steps:

(a) before installing the sensors on the cart, the sensor outputs are soldered to the blocks to prevent electrical contact with the surface of the cart;
(b) the installation site is treated (wiped) with acetone in order to degrease the surface. It is also necessary to wipe the glued (lower part) surface of the sensor with acetone;
(c) glue is applied to the sensor (second glue moment is universal);
(d) next, the sensor must be strongly pressed against the surface previously prepared for installation [12]. It is important during the installation of the sensor to avoid the occurrence of air and bubbles between the sensor and the surface to be glued, it is necessary to press the sensor completely against the surface and hold for at least 30 seconds.

The dynamic performance of the diesel locomotive was measured simultaneously with measurements to determine the level of impact of the diesel locomotive on the track and turnouts [13].

Figure 2. Installation of strain gauges on the side bearings of the locomotive bogie.

3. Dynamic performance of a diesel locomotive on turnouts

The dynamic performance of the diesel locomotive on turnouts was determined by measurements made when the diesel locomotive was passing turnout's No. 13 of grade 1/9 and No.

Preprints (www.preprints.org) | NOT PEER-REVIEWED | Posted: 7 September 2023 doi:10.20944/preprints202309.0483.v1

29 of grade 1/11 on rails R65 located at the station Belle. The direction when the locomotive CKD6E-2108 moved with the 1st wheel pair forward from the station towards the entrance switches was taken as the direct course of the diesel locomotive [14]. Figure 3 shows the oscillograms of the primary measurements of dynamic processes recorded at turnouts. The frame forces were determined as the product of the transverse displacements of the wheelset relative to the bogie frame and the stiffness of their connection. When processing processes, the quasi-static component was taken into account. The estimated values of the processed process were determined as the arithmetic average of the three largest measured values at one speed [15]. The dependence of the ratio of frame to static load from the wheelset on the rails on the speed of movement is shown in Figures 3 and 4.

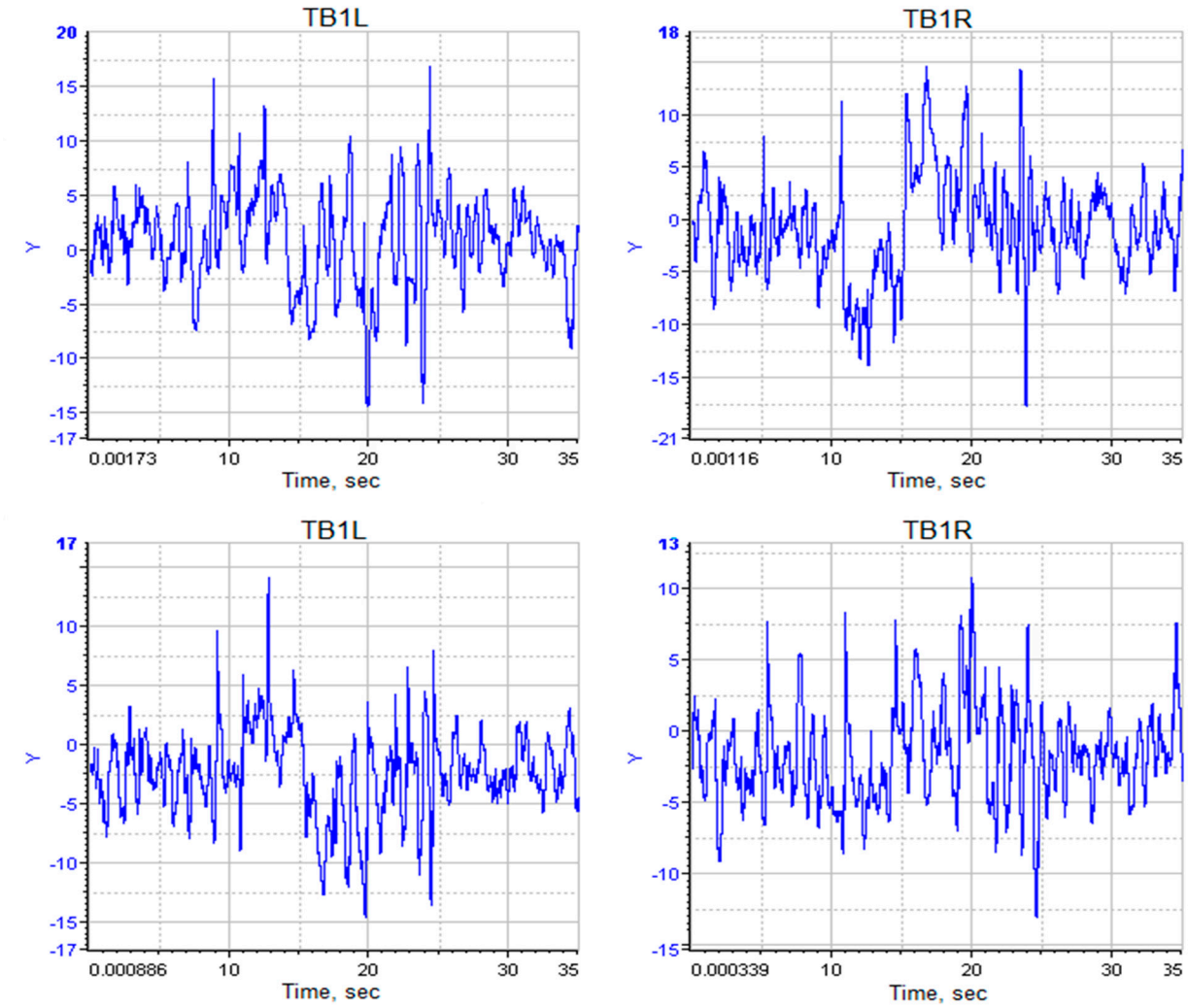

Figure 3. Vertical movements of the bogie frame relative to the wheelset of the locomotive CKD6E-2108 when moving along turnouts, mm.

Preprints (www.preprints.org) | NOT PEER-REVIEWED | Posted: 7 September 2023 doi:10.20944/preprints202309.0483.v1

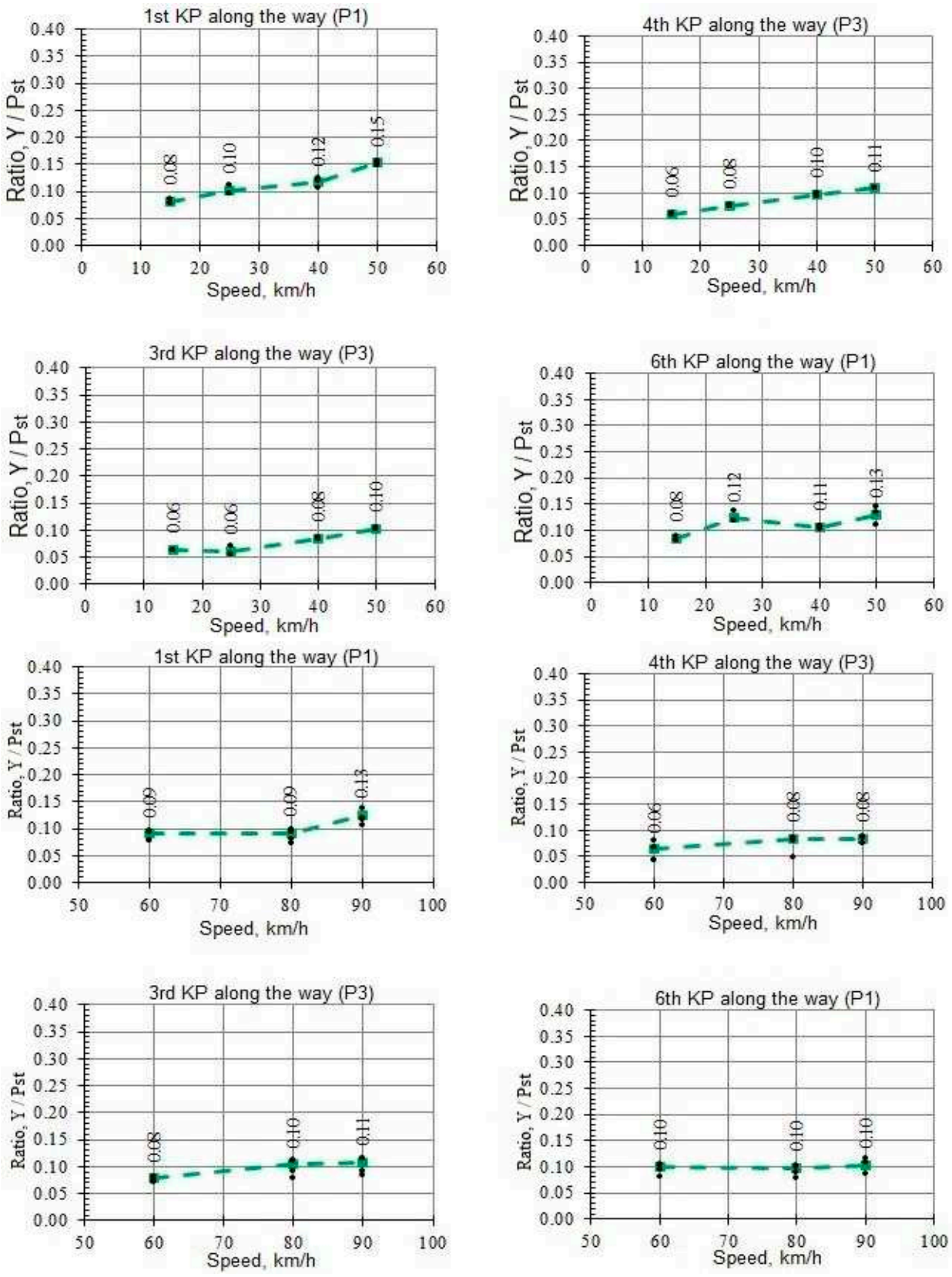

Figure 4. The ratio of frame forces to the static load from the wheelset on the rails on the CKD6E-2108 diesel locomotive when driving on turnout's P65 grade 1/9 and 1/11 on the side.

Preprints (www.preprints.org) | NOT PEER-REVIEWED | Posted: 7 September 2023 doi:10.20944/preprints202309.0483.v1

Figures 4 and 5 show that the ratio of frame forces to the static load from the wheelset on the rails is within the allowable range [16]. In the considered range of speeds, when the CKD6e-2108 diesel locomotive passes the turnouts P65 of grade 1/9 and 1/11, this indicator does not exceed 0.31 when moving sideways and 0.15 when moving in a straight line [17]. Thus, the frame forces of the diesel locomotive during the passage of turnouts P65 grades 1/9 and 1/11 meet the requirements in the entire range of speeds at which the tests were carried out. Based on the instantaneous values of the frame forces and the coefficient of vertical dynamics of the first stage of the spring suspension, the values of the stability factor against wheel derailment were calculated (hereinafter in the Figures and Tables - KZU). The minimum value of the stability factor against wheel derailment when passing turnouts is summarized in Tables 1 and 2.

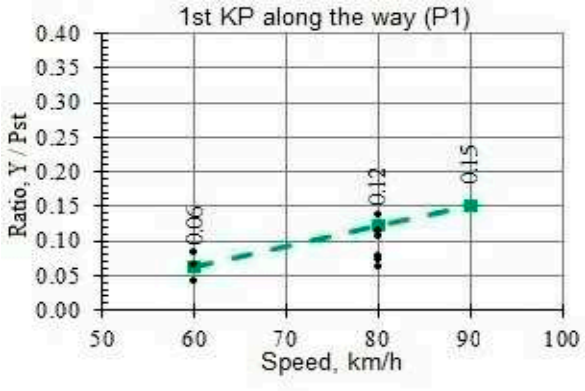

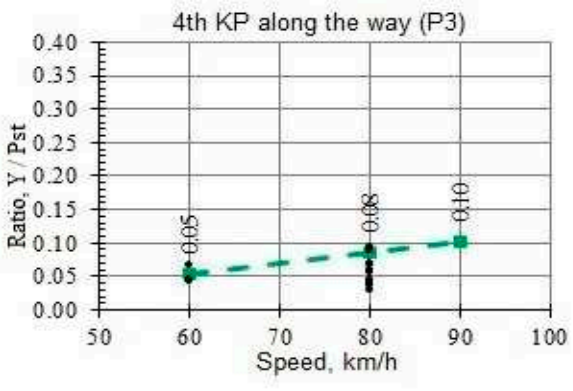

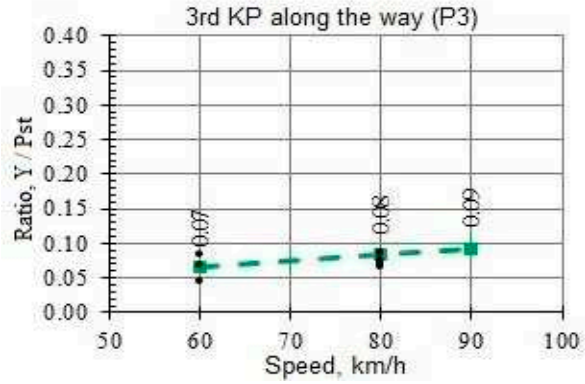

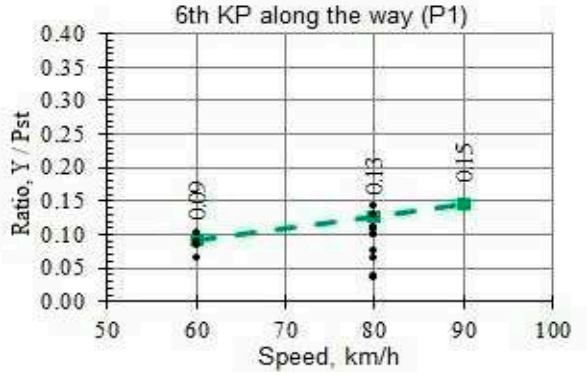

Preprints (www.preprints.org) | NOT PEER-REVIEWED | Posted: 7 September 2023 doi:10.20944/preprints202309.0483.v1

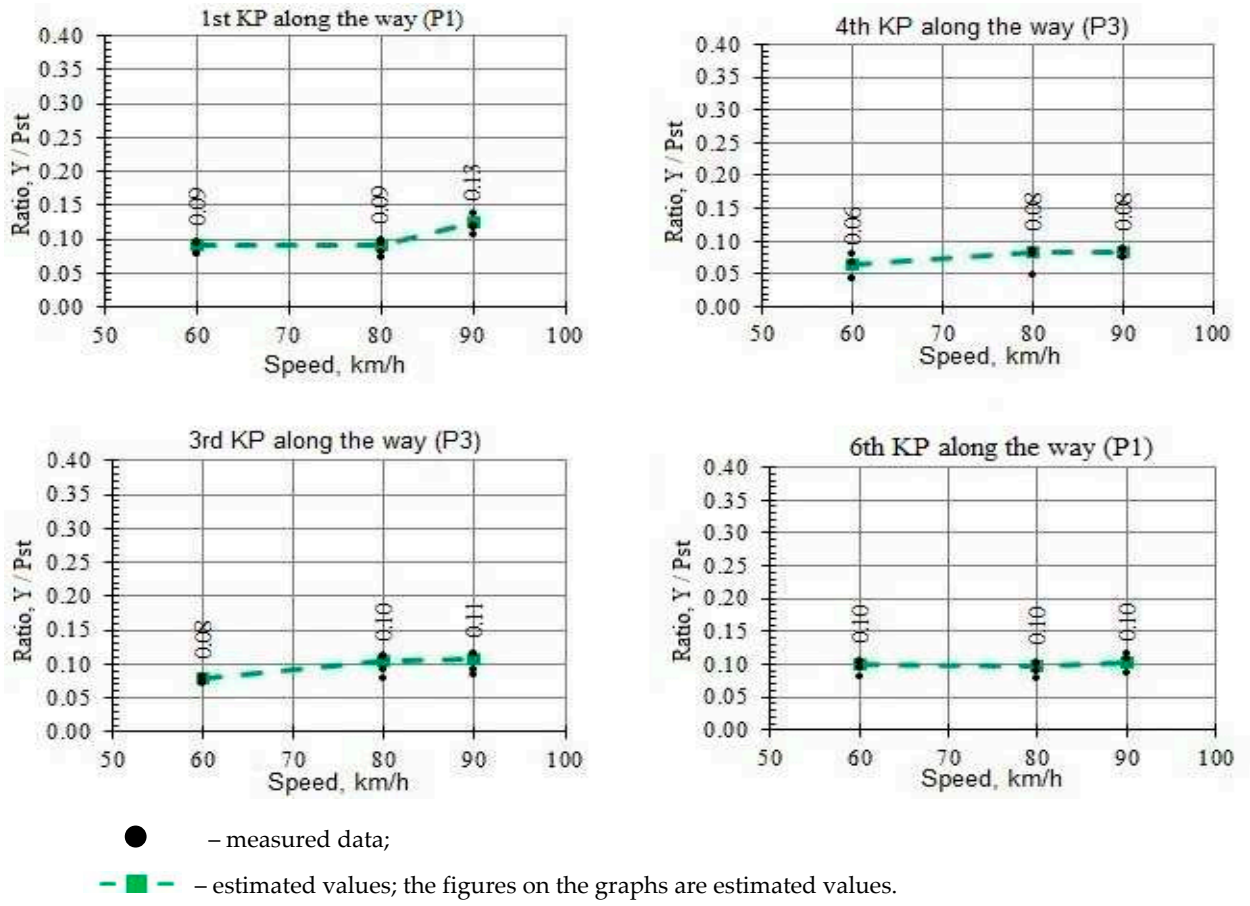

Figure 5. The ratio of frame forces to the static load from the wheelset on the rails on the CKD6E-2108 diesel locomotive when driving on turnout's P65 grades 1/9 and 1/11 in a straight line.

Table 1. Stability factor against wheel derailment in turnouts with a 1/9 cross.

Direction of travel	**Minimum KZU value**						
	sideways movement				**straight line**		
	speed, km/h						
	15	25	40	50	60	80	90
forward	2,49	2,47	2,43	2,24	2,83	2,73	2,71
Reverse	2,51	2,72	2,59	2,27	2,61	2,70	2,59
Allowed value	1,4						

Table 2. Stability factor against wheel derailment in turnouts with a crosspiece of brand 1/11.

Direction of travel	**Minimum KZU value**						
	sideways movement				straight line		
	speed, km/h						
	15	25	40	50	60	80	90
forward	2,86	2,68	2,78	2,45	2,85	2,68	2,60
Reverse	2,76	2,59	2,59	2,52	2,75	2,49	2,36
Allowed value	1,4						

The obtained dependencies of the stability factor against derailment of the wheel from the rail speed are shown in Figures 6 and 7.

Preprints (www.preprints.org) | NOT PEER-REVIEWED | Posted: 7 September 2023 doi:10.20944/preprints202309.0483.v1

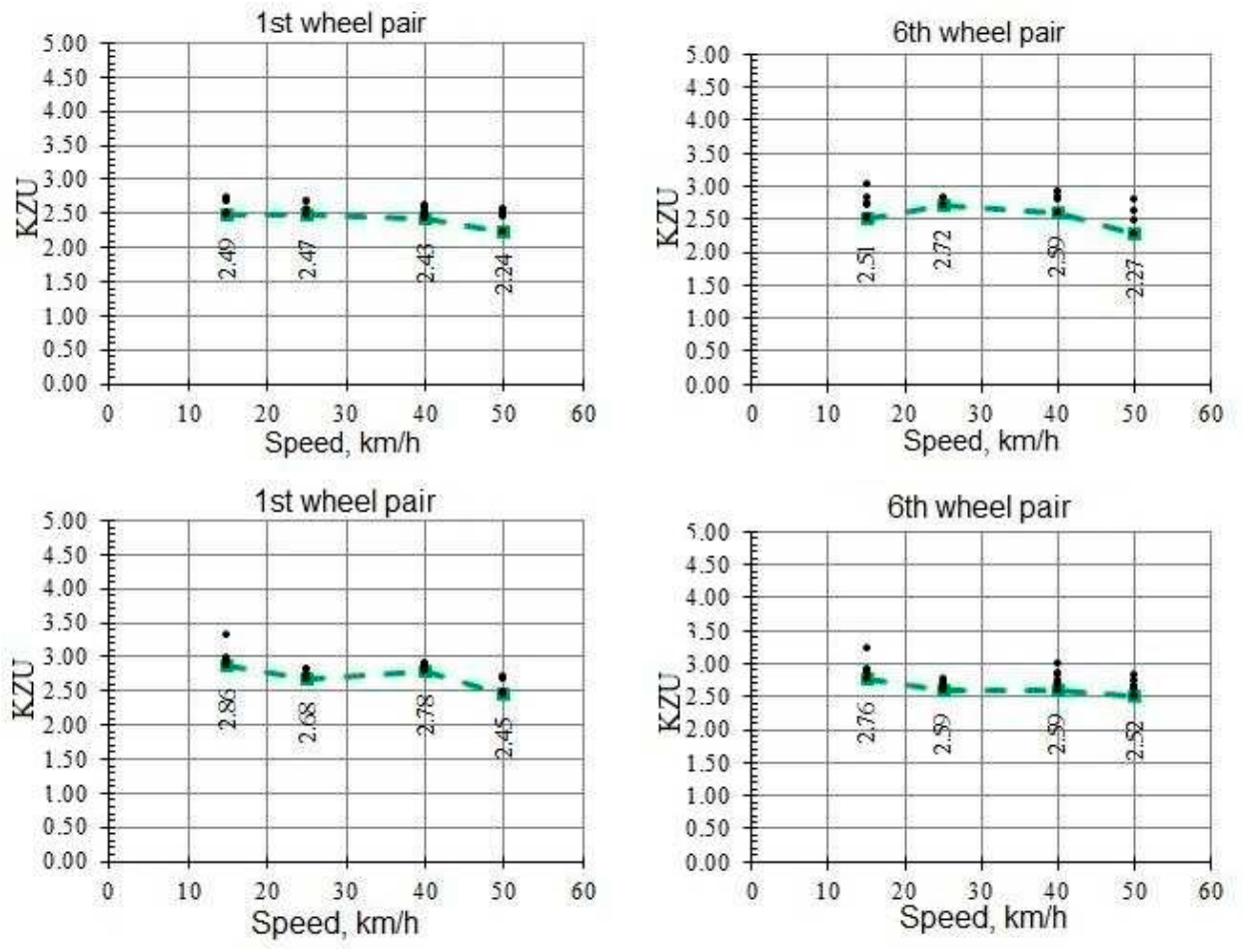

Figure 6. Stability factor against wheel derailment when passing a turnout with a 1/9 and 1/11 crosspiece on its side.

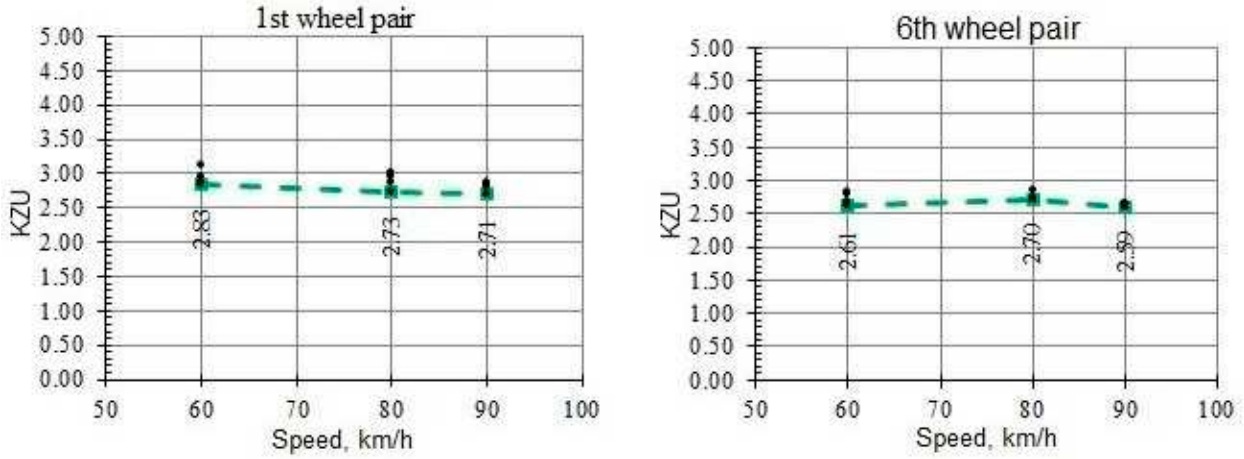

Preprints (www.preprints.org) | NOT PEER-REVIEWED | Posted: 7 September 2023 doi:10.20944/preprints202309.0483.v1

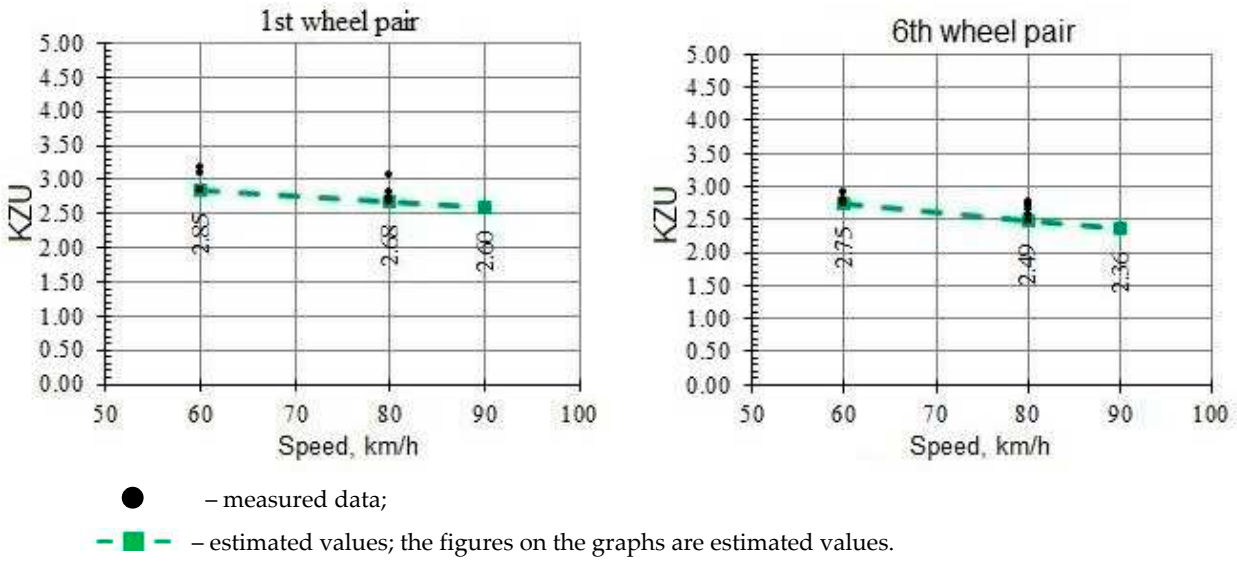

Figure 7. Stability factor against wheel derailment when passing a turnout with a crosspiece of brand 1/9 and 1/11 in a straight direction.

The data given in Tables 1 and 2 and Figures 6 and 7 show that the stability factor against wheel derailment when the locomotive passes turnouts on its side up to a speed of 50 km/h and in a straight direction up to 90 km/h are in acceptable limits, i.e. take values of at least 1.4. The results show that the dynamic performance of the diesel locomotive when passing turnouts meets the requirements of the "Norms for Permissible Speeds of Locomotives and Wagons on Railway Tracks of Gauge 1520 (1524) mm of Railway Transport of the Republic of Kazakhstan" (hereinafter referred to as the Norms for Permissible Speeds) [18]. Consequently, the speed of movement on the turnouts in accordance with the Norms of permissible speeds of movement according to the assessment of dynamic indicators is limited to 40 km/h when moving on the turnouts on the side and the design speed when driving on the turnouts in the forward direction [19].

4. Dynamic performance of a diesel locomotive on a straight section of the track

Before testing, a track measuring car was passed through this section. Based on the results of the measurements, the maximum allowable speed was set at 90 km/h.

Figure 8. Installation of strain gauges on the side neck of the rail.

 doi:10.20944/preprints202309.0483.v1

Figure 9. Installation of load cells on the rail foot.

For the direct course of the diesel locomotive, the direction was taken when the CKD6E-2108 diesel locomotive moved forward with the 1st wheel pair [20]. The coefficient of vertical dynamics of the first stage of the spring suspension was determined as the ratio of the dynamic vertical displacement of the bogie relative to the wheelset (axle box), registered during the movement of the diesel locomotive, to the vertical static deflection of the first stage, which is 123 mm for the CKD6e diesel locomotive [21]. The coefficient of vertical dynamics of the second stage of the spring suspension was determined as the ratio of the values of the dynamic signal recorded by tensometric circuits to the value of the signal obtained during static tests.

Based on the results of data processing at a given speed, separate data arrays were formed for each sensor. According to these arrays, the estimated values of the coefficient of vertical dynamics of the first stage of the spring suspension were found [22]. Dynamic vertical movements were processed without taking into account the quasi-static component. All measurements were divided into speeds and directions of movement. In each race, one maximum amplitude value of the dynamic process was selected.

Similarly, data processing was carried out to determine the coefficient of vertical dynamics of the second stage of the spring suspension. Frame forces were processed by the method described earlier.

Figures 10–12 show oscillograms of primary measurements of dynamic processes recorded while driving along a straight section.

Figure 14 shows the graphs of the dependence of the coefficient of vertical dynamics of the first stage of the spring suspension on the speed when the diesel locomotive passes along a straight section of the track.

Figure 15 shows the graphs of the dependence of the coefficient of vertical dynamics of the second stage of the spring suspension on the speed when the diesel locomotive passes along a straight section of the track.

Figure 16 shows the graphs of the ratio of frame forces to the static load from the wheelset on the rails on the speed when the diesel locomotive passes along a straight section of the track.

The data of Figures 13 and 14 show that the values of the coefficients of vertical dynamics of the first and second stages of the spring suspension of the CKD6E-2108 diesel locomotive do not exceed the permissible limits [23]. The maximum values for the coefficients of vertical dynamics were 0.11 for the first stage and 0.25 for the second stage. It is worth noting that the limit value of 0.25 for the vertical dynamics coefficient of the second stage was obtained when driving at a speed of 90 km/h, i.e. 12.5% higher than design speed [24].

The maximum value of the ratio of frame forces to the static load from the wheelset on the rails was 0.08.

Preprints (www.preprints.org) | NOT PEER-REVIEWED | Posted: 7 September 2023 doi:10.20944/preprints202309.0483.v1

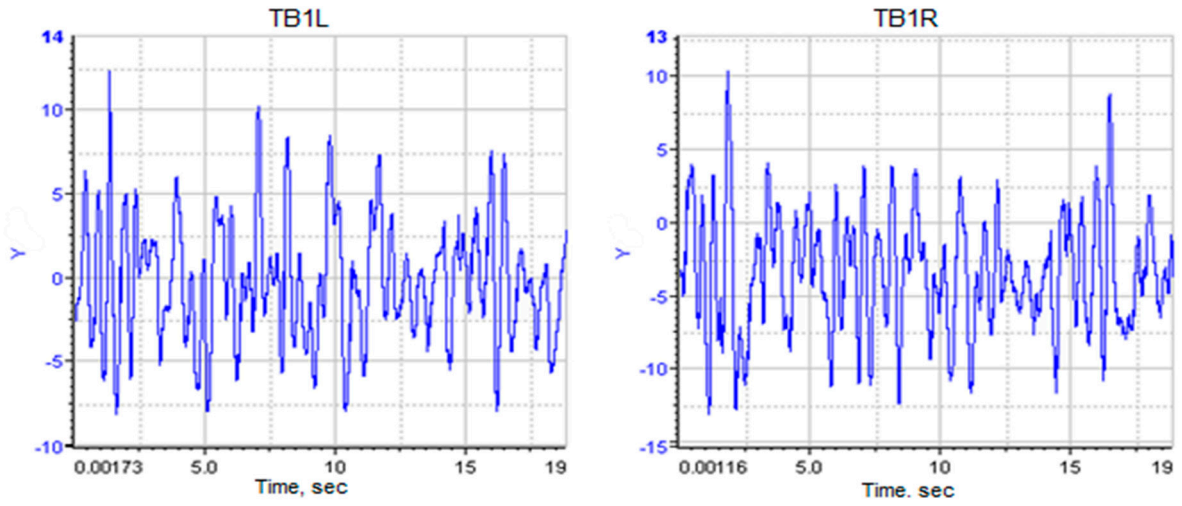

Figure 10. Vertical movements of the bogie frame relative to the wheelset of the CKD6E-2108 diesel locomotive when moving along a straight section of track, mm.

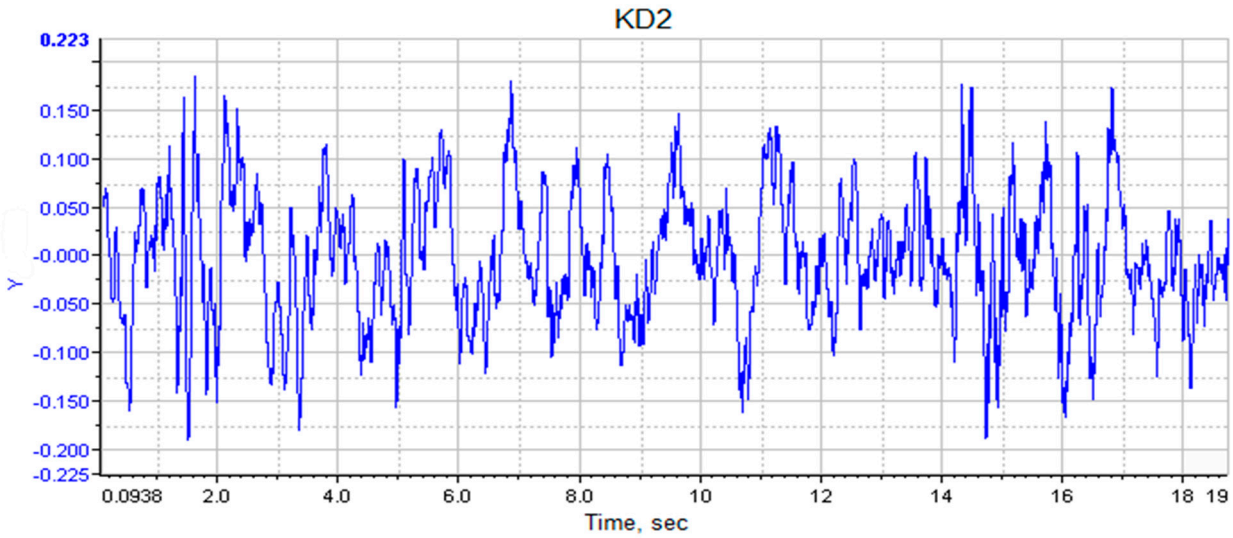

Figure 11. The coefficient of vertical dynamics of the second stage of the spring suspension of the CKD6E-2108 diesel locomotive when moving along a straight section of the track.

Preprints (www.preprints.org) | NOT PEER-REVIEWED | Posted: 7 September 2023 doi:10.20944/preprints202309.0483.v1

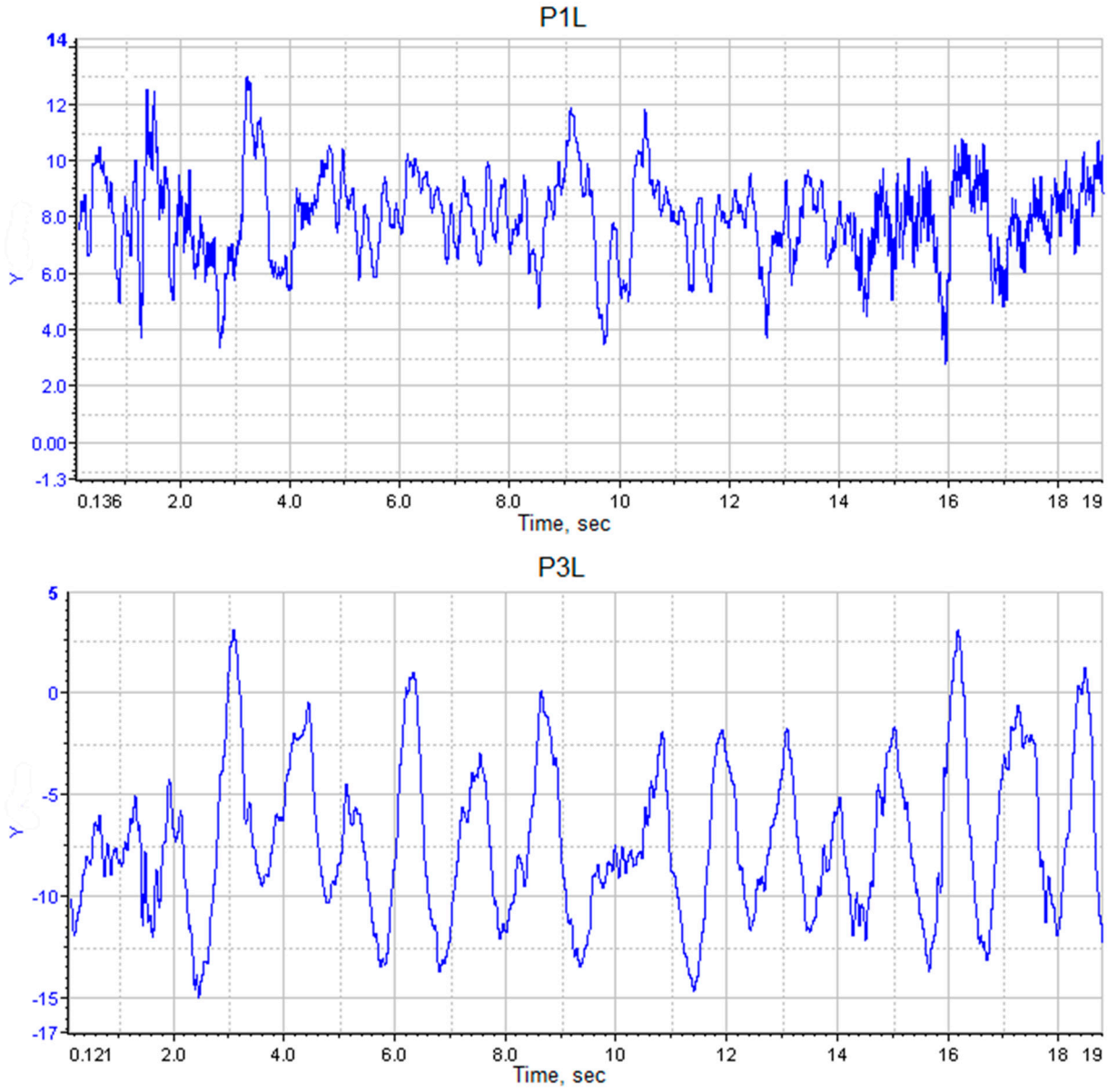

Figure 12. Frame forces on a CKD6E-2108 diesel locomotive when moving along a straight section of track.

Preprints (www.preprints.org) | NOT PEER-REVIEWED | Posted: 7 September 2023 doi:10.20944/preprints202309.0483.v1

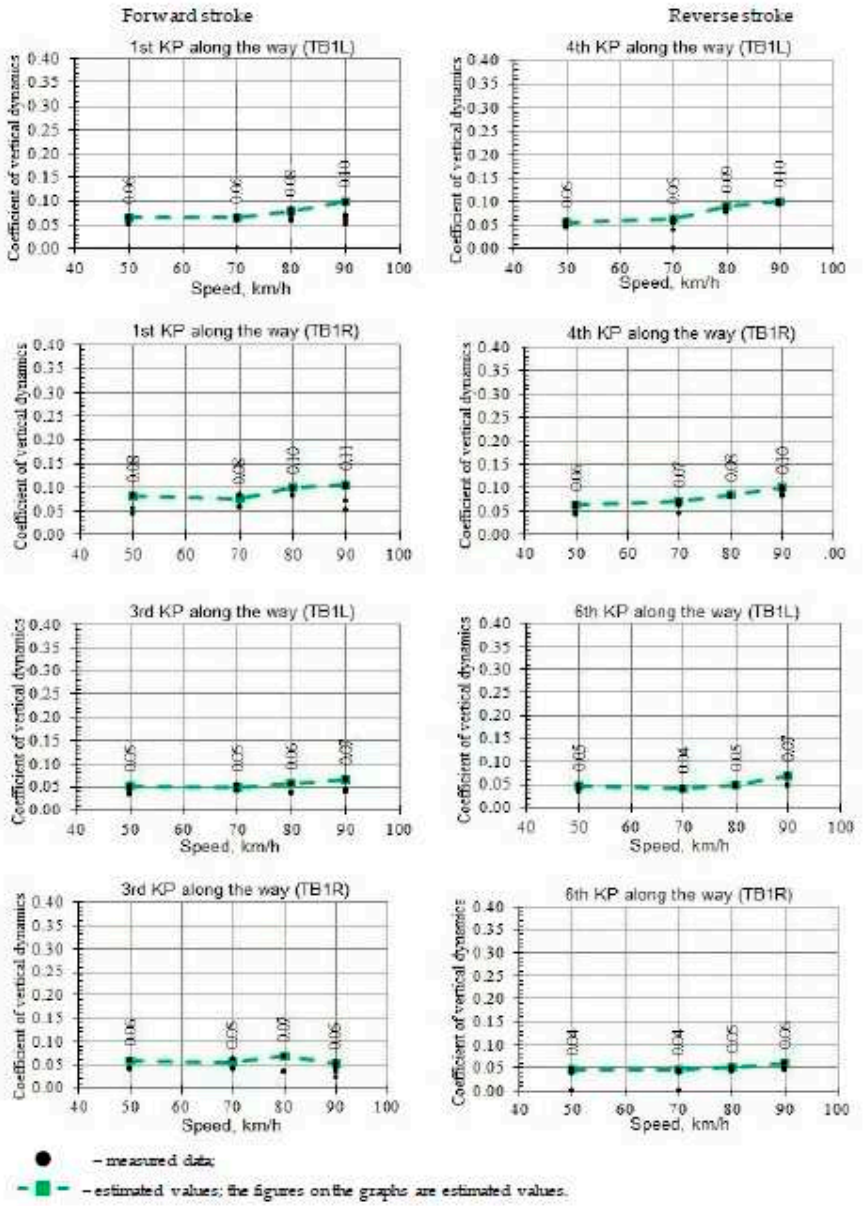

Figure 13. Coefficient of vertical dynamics of the first stage of the spring suspension of the CKD6E-2108 diesel locomotive when moving along a straight section of the track.

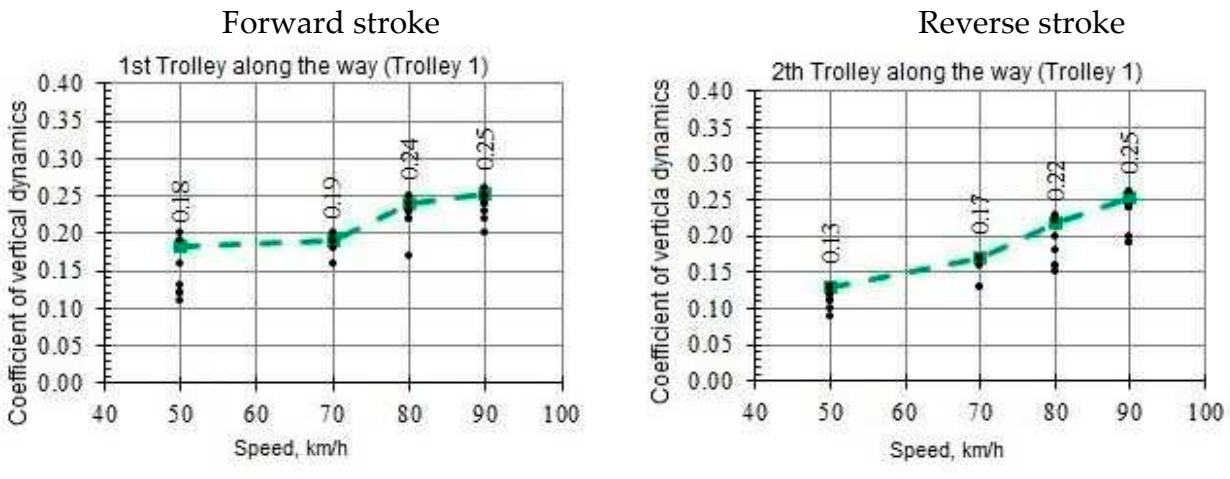

Preprints (www.preprints.org) | NOT PEER-REVIEWED | Posted: 7 September 2023 doi:10.20944/preprints202309.0483.v1

– estimated values; the figures on the graphs are estimated values.

Figure 14. The coefficient of vertical dynamics of the second stage of the spring suspension of the CKD6E-2108 diesel locomotive when moving along a straight section of the track.

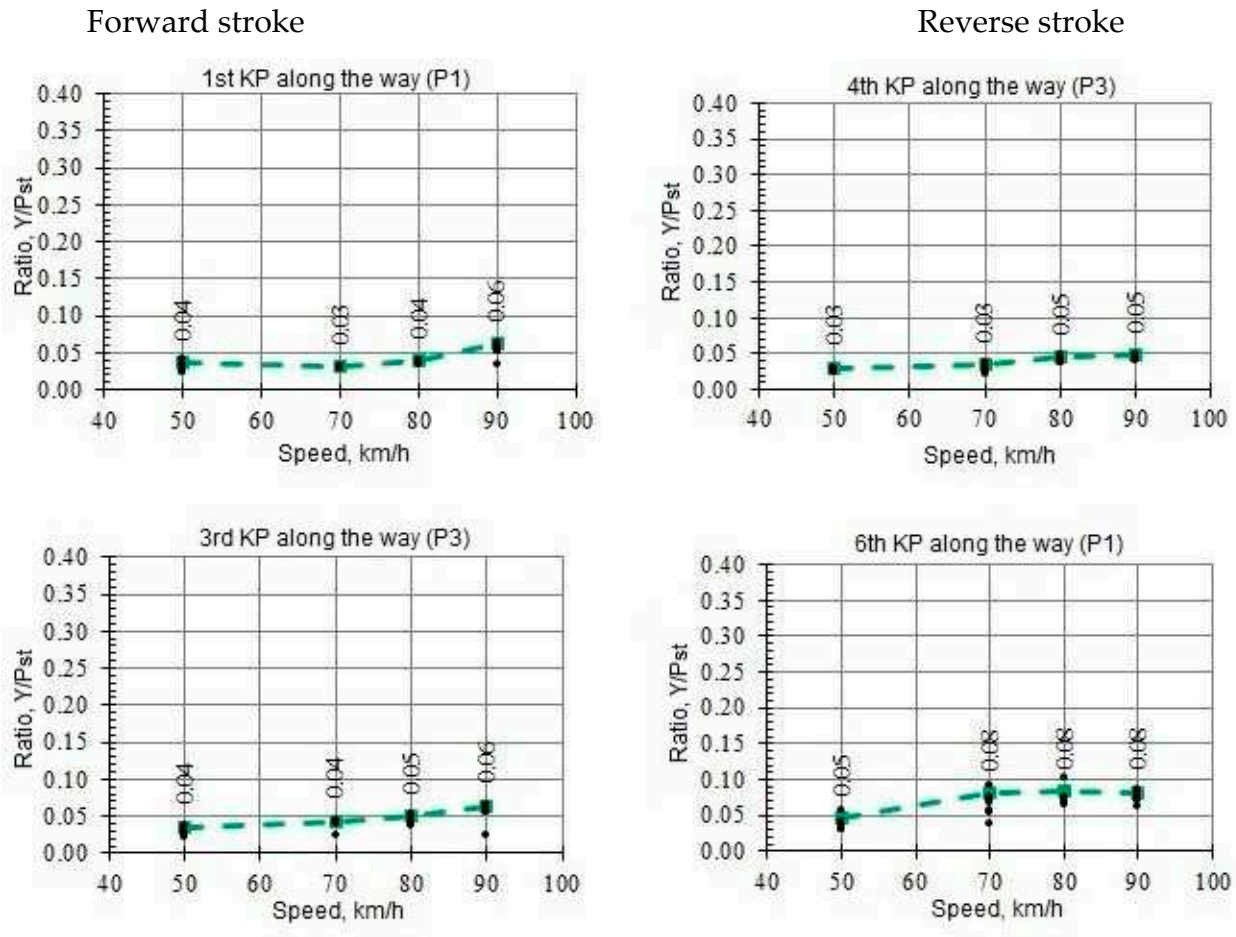

– measured data;

– estimated values; the figures on the graphs are estimated values.

Figure 15. The ratio of frame forces to the static load from the wheelset on the rails on the CKD6E-2108 diesel locomotive when moving along a straight section of track.

Figure 16 shows the dependence of the stability factor against derailment of the wheel from the speed of movement, built on the basis of the results given in Table 3. The minimum values of the stability factor against derailment calculated from the data recorded on the straight section of the track are shown in Table 3.

Preprints (www.preprints.org) | NOT PEER-REVIEWED | Posted: 7 September 2023 doi:10.20944/preprints202309.0483.v1

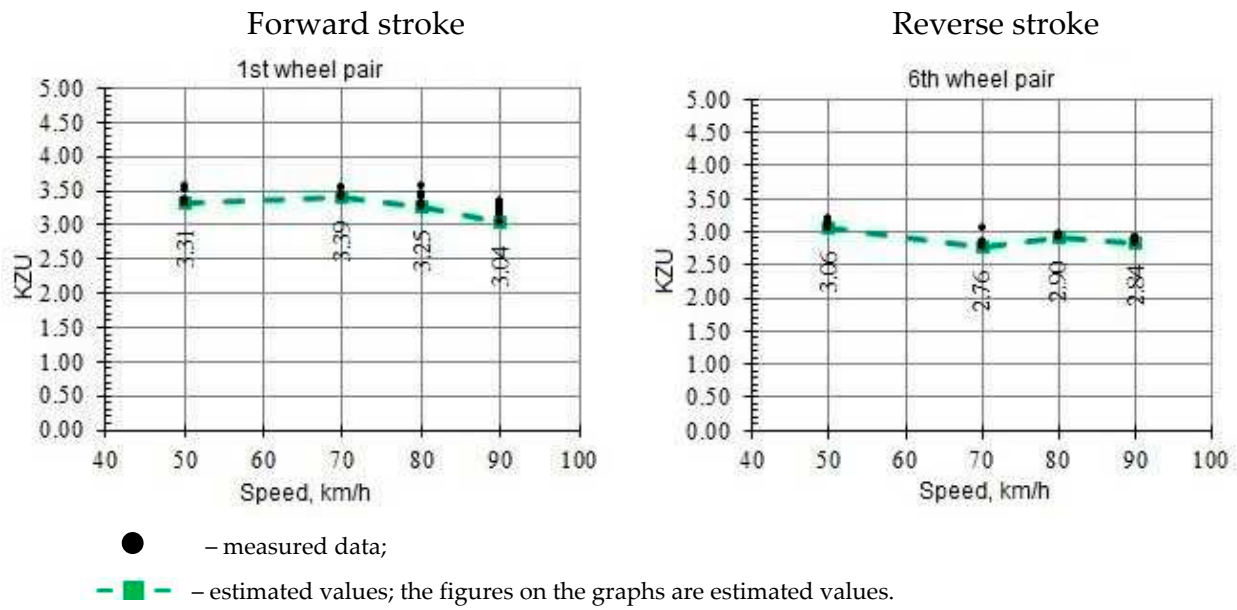

Figure 16. Stability factor against wheel derailment on a straight section of the track.

Table 3. Stability factor against wheel derailment on a straight section of the track.

Direction of travel	Minimum value of KZU, at speed, km/h			
	50	70	80	90
forward stroke	3,31	3,39	3,25	3,04
Reverse stroke	3,06	2,76	2,90	2,84
Allowed value	1,4			

As can be seen from Figure 16 and Table 3, the minimum value of the stability factor against wheel derailment on a straight section of the track is significantly higher than the standard value. Thus, the speed of movement along straight sections in accordance with the Norms of permissible movement speeds according to the assessment of dynamic indicators is limited by the design speed [25].

5. Dynamic performance in a curve with a radius of 400 m

Before testing, a track measuring car was passed through this section. According to the results of measurements, the maximum permissible speed of movement was set at 85 km/h.

The data for determining the estimated values of the frame forces, the coefficients of vertical dynamics of the first and second stages of suspension were processed in the same way as for the previous sections [26]. Figures 17–19 show oscillograms of primary measurements of dynamic processes recorded while moving in a curve with a radius of 400 m. The processing results are shown in Figures 20–22.

Preprints (www.preprints.org) | NOT PEER-REVIEWED | Posted: 7 September 2023 doi:10.20944/preprints202309.0483.v1

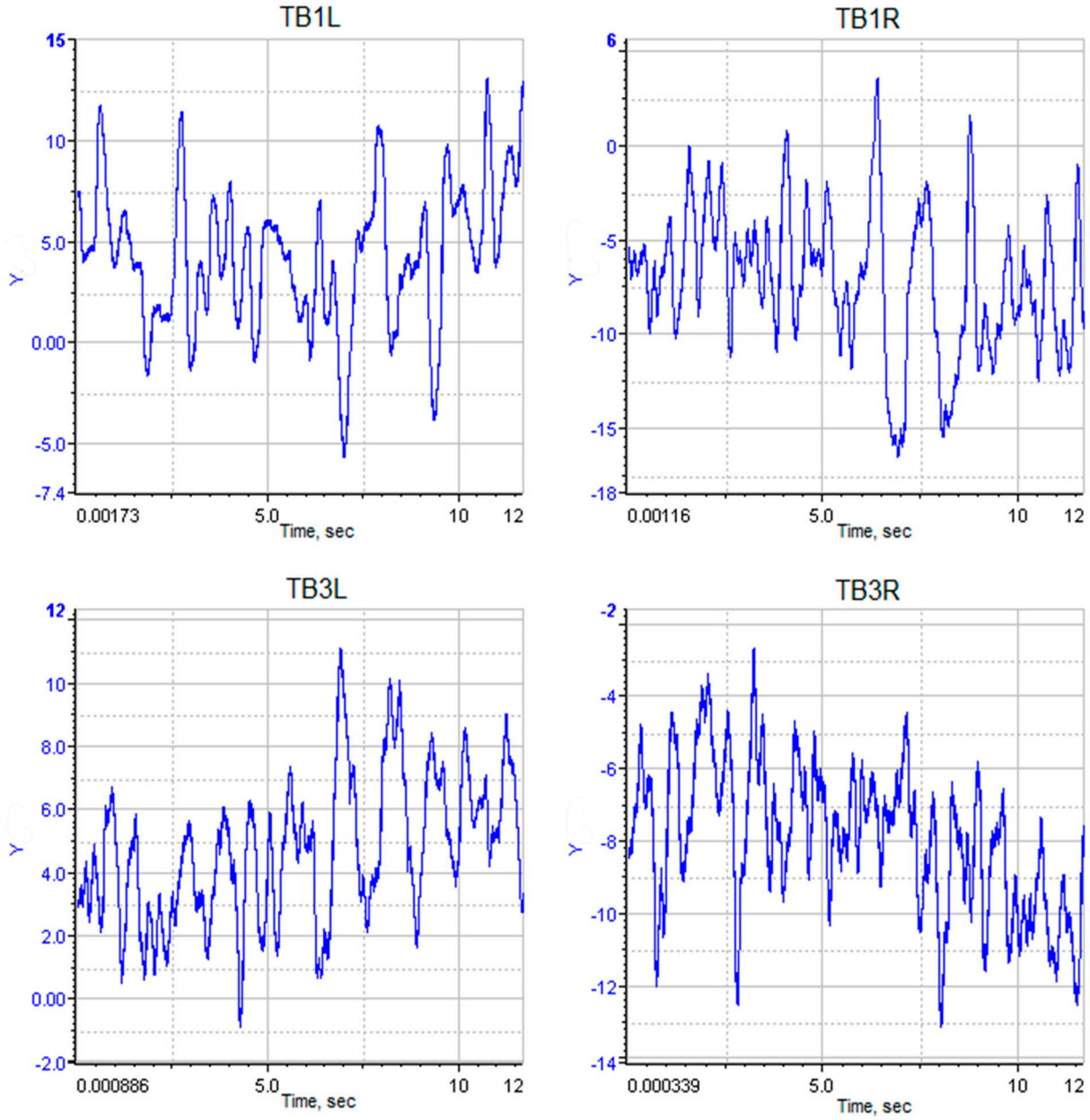

Figure 17. Vertical movements of the bogie frame relative to the wheelset of the CKD6E-2108 diesel locomotive when moving in a curve with a radius of 400 m.

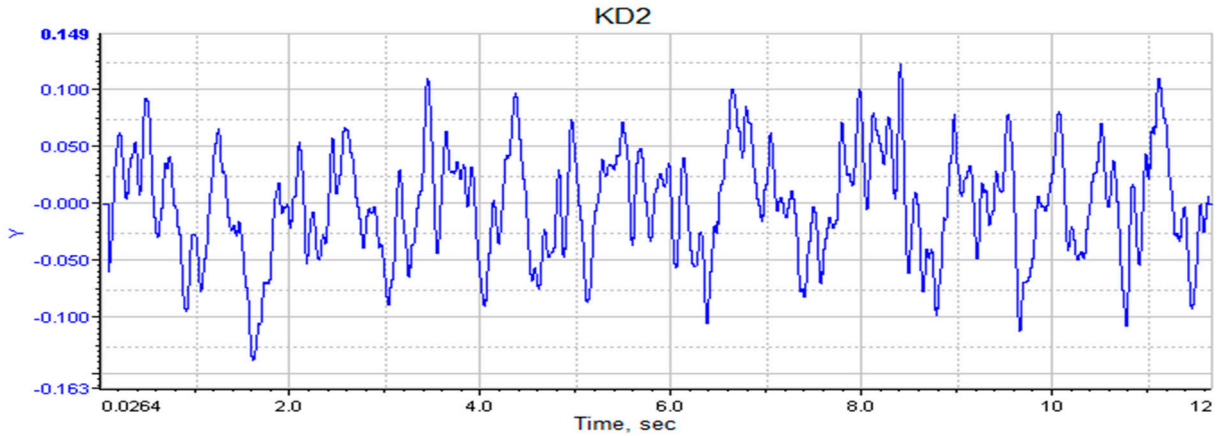

Preprints (www.preprints.org) | NOT PEER-REVIEWED | Posted: 7 September 2023 doi:10.20944/preprints202309.0483.v1

Figure 18. The coefficient of vertical dynamics of the second stage of the spring suspension of the CKD6E-2108 diesel locomotive when moving in a curve with a radius of 400 m.

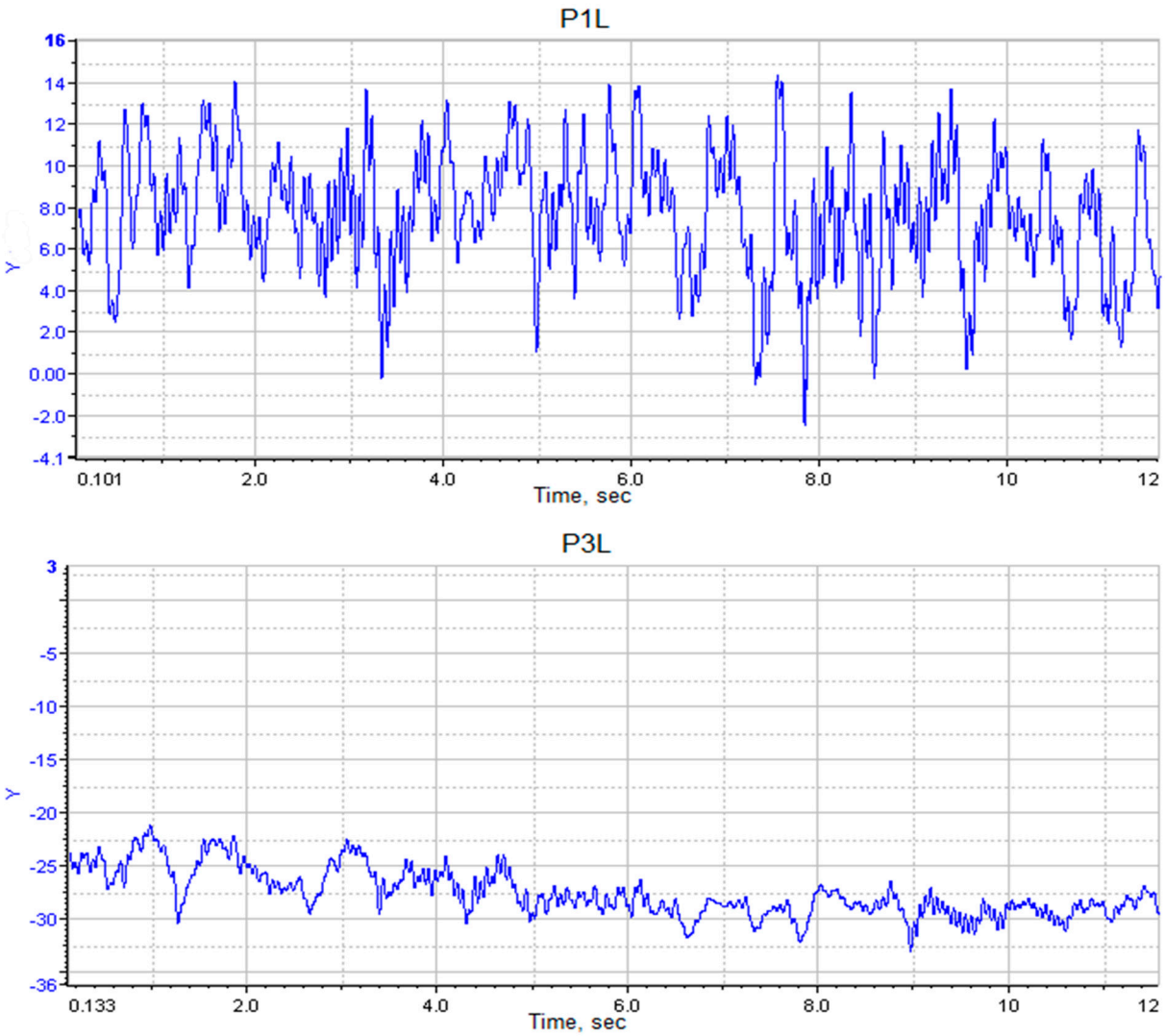

Figure 19. Frame forces on a CKD6E-2108 diesel locomotive when moving in a curve with a radius of 400 m.

Preprints (www.preprints.org) | NOT PEER-REVIEWED | Posted: 7 September 2023 doi:10.20944/preprints202309.0483.v1

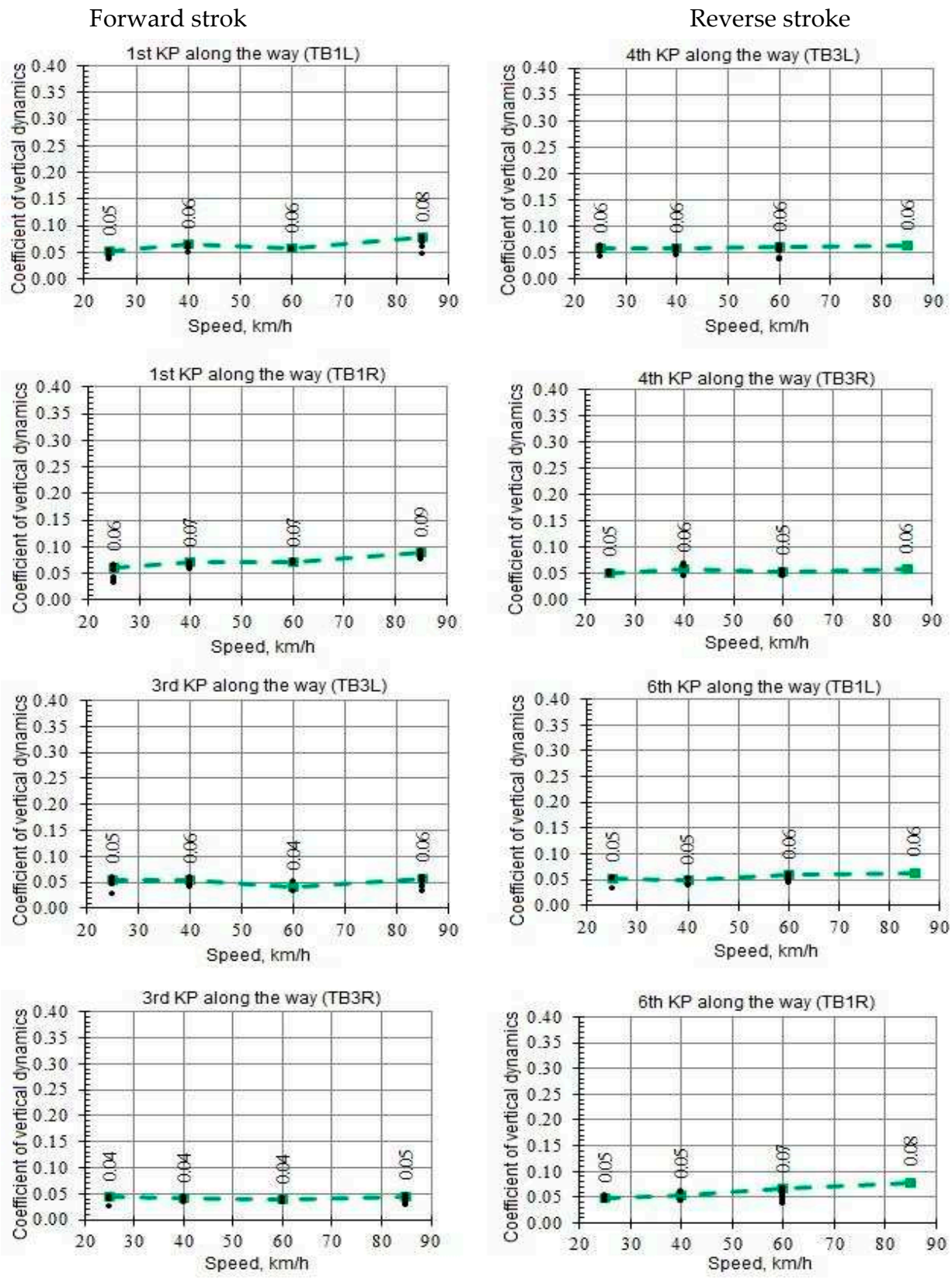

Figure 20. The coefficient of vertical dynamics of the first stage of the spring suspension of the CKD6E-2108 diesel locomotive when moving in a curve with a radius of 400 m.

Preprints (www.preprints.org) | NOT PEER-REVIEWED | Posted: 7 September 2023 doi:10.20944/preprints202309.0483.v1

Forward stroke

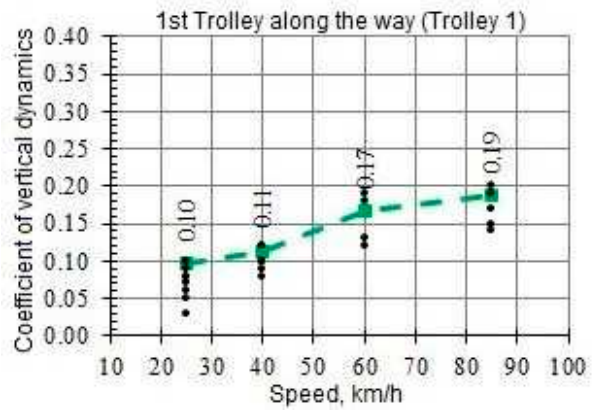

Reverse stroke

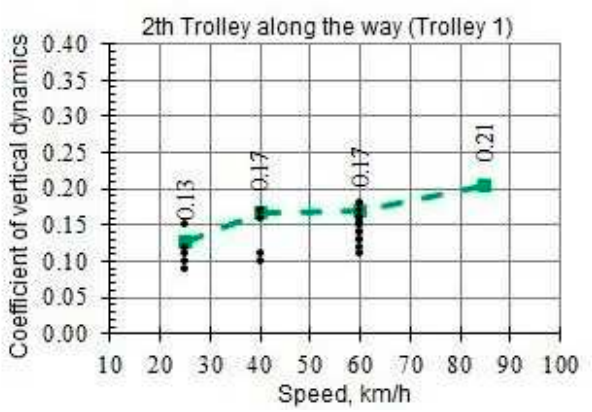

● – measured data;

– ■ – – estimated values; the figures on the graphs are estimated values.

Figure 21. The coefficient of vertical dynamics of the second stage of the spring suspension of the CKD6E-2108 diesel locomotive when moving in a curve with a radius of 400 m.

Forward stroke

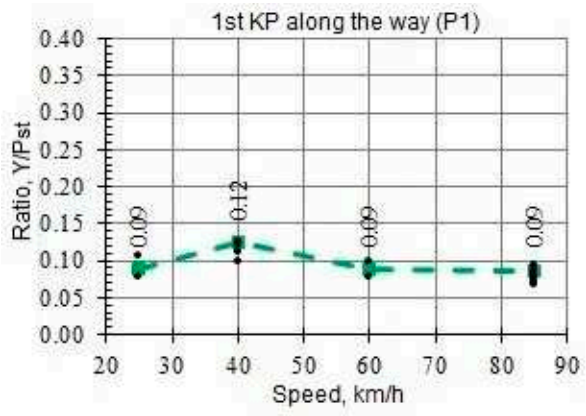

Reverse stroke

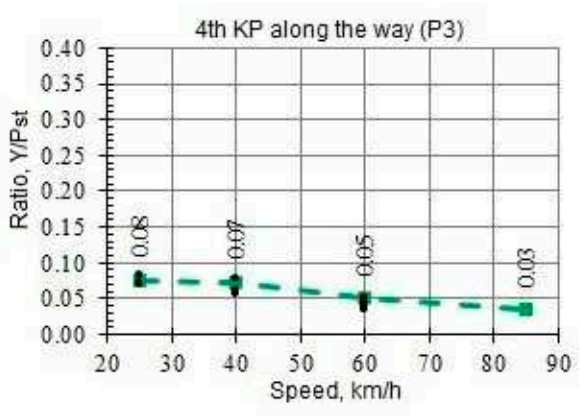

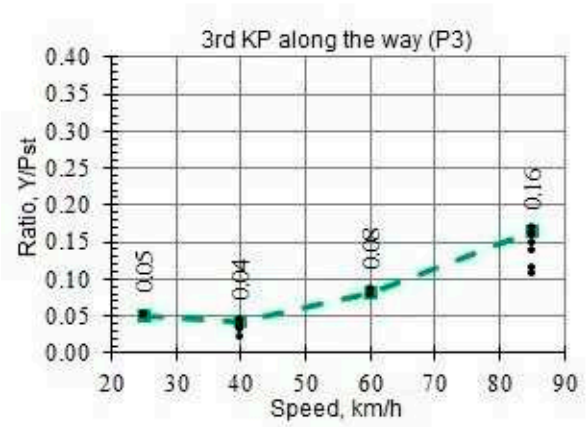

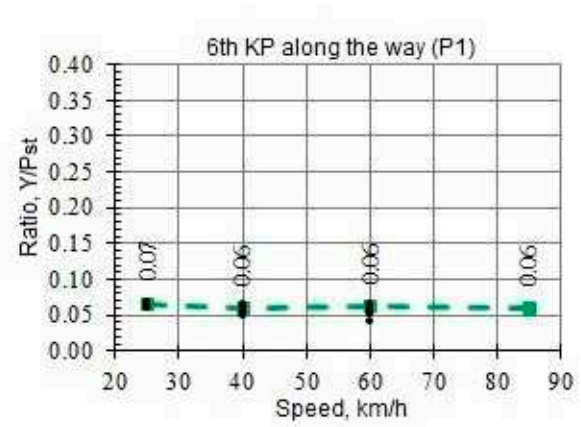

● – measured data;

– ■ – – estimated values; the figures on the graphs are estimated values.

Figure 22. The ratio of frame forces to the static load from the wheelset on the rails on the CKD6E-2108 diesel locomotive when moving in a curve with a radius of 400 m.

Preprints (www.preprints.org) | NOT PEER-REVIEWED | Posted: 7 September 2023 doi:10.20944/preprints202309.0483.v1

The minimum values of the stability factor against wheel derailment calculated from the data recorded when driving in a curve with a radius of 400 m are shown in Table 4.

Table 4. Stability factor against wheel derailment when moving in a curve with a radius of 400 m.

Minimum value of KZU, at speed, km/h				
Direction of travel	25	40	60	85
forward stroke	3,20	3,28	3,48	3,12
reverse stroke	3,05	3,11	3,04	3,05
Allowed value	1,4			

Figure 23 shows the dependence of the stability factor against wheel derailment on the speed of movement [27].

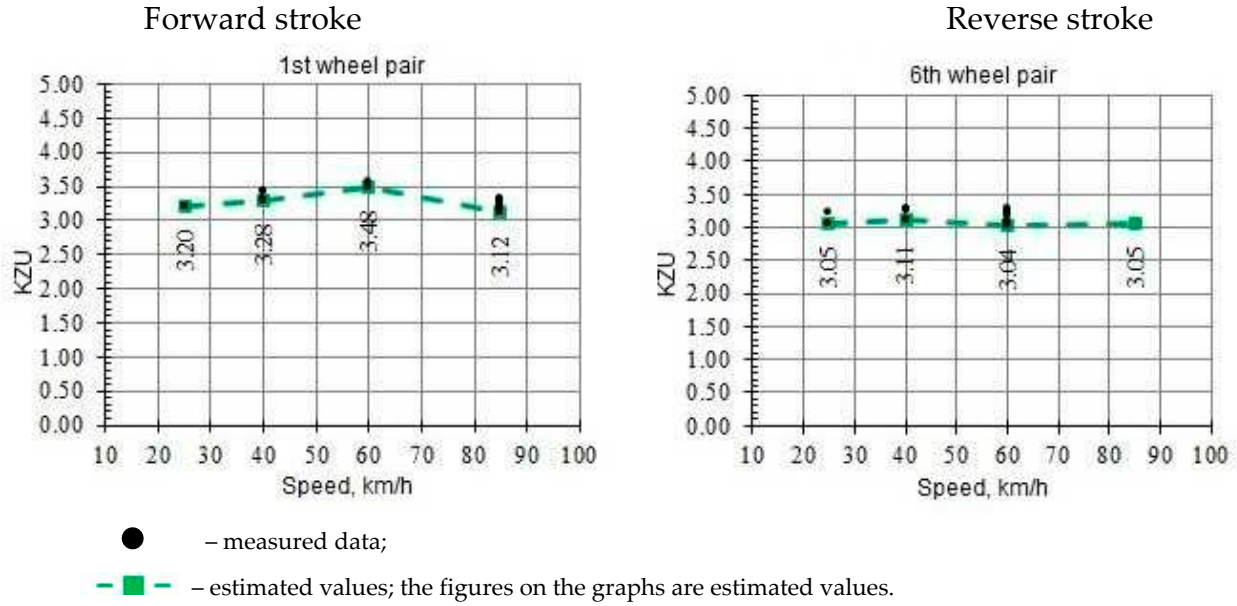

Figure 23. Safety factor against wheel derailment in a curve with a radius of 400 m.

The results shown in Figures 20–22 show that the dynamic performance of the locomotive: the ratio of frame forces to the static load from the wheelset on the rails, the vertical dynamics coefficients of the first and second suspension stages and the stability factor against wheel derailment recorded on the track section in a curve with a radius of 400 m meet the requirements [28]. The speeds of movement along curves of a small radius in accordance with the Norms of permissible movement speeds according to the assessment of dynamic indicators are limited based on the condition of not exceeding the outstanding acceleration of 0.7 m/s^2, as well as the design speed.

6. Drawing up equations of vertical oscillations of a diesel locomotive

When compiling the mathematical model of oscillations of the undercarriage, a flat design scheme of the locomotive was adopted (see Figure 24). Equations of steady-state spatial vertical oscillations of the vehicle-track system under study with respect to the complex amplitudes of generalized coordinates, compiled taking into account the accepted assumptions and describing forced oscillations in the longitudinal vertical plane [29].

Preprints (www.preprints.org) | NOT PEER-REVIEWED | Posted: 7 September 2023 doi:10.20944/preprints202309.0483.v1

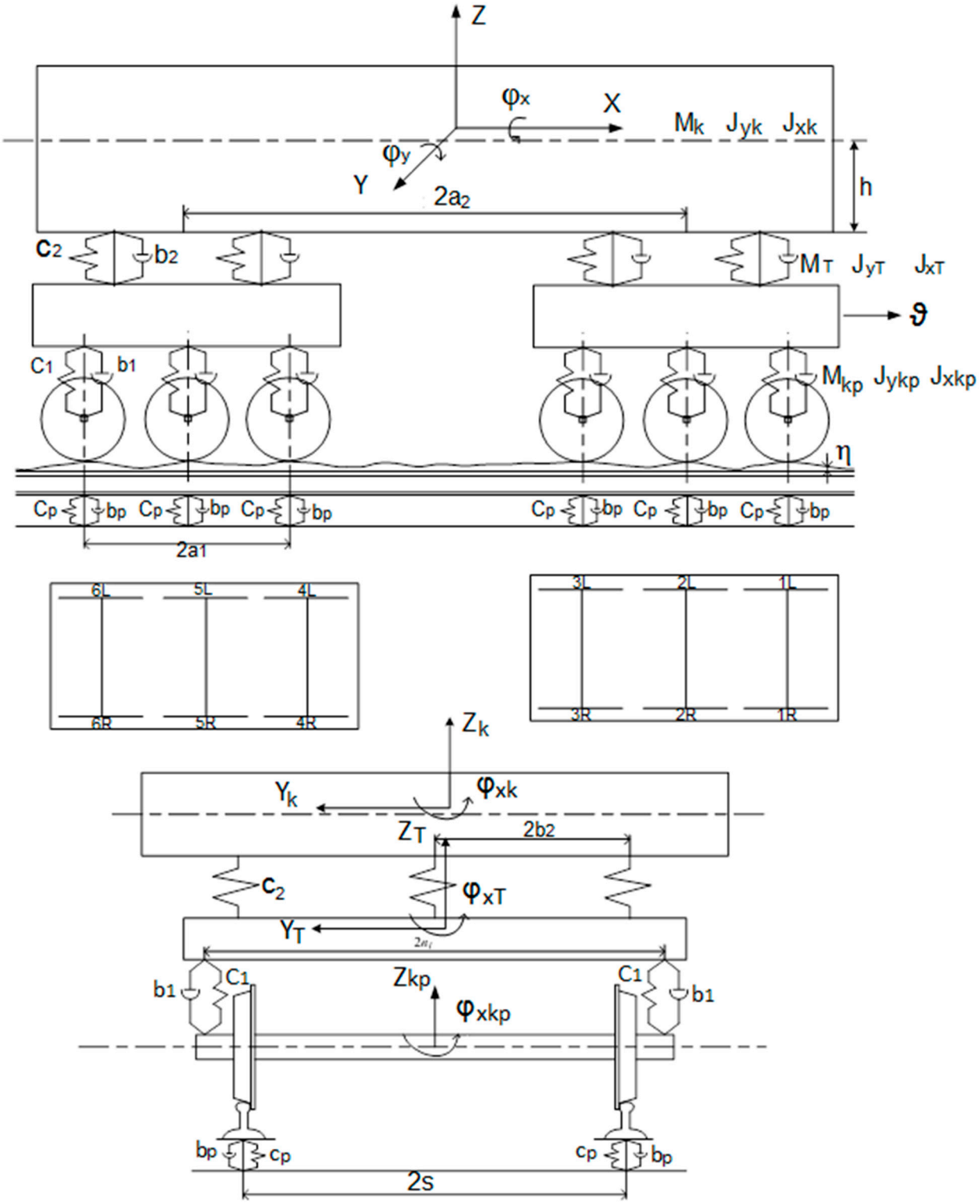

Figure 24. Kinematic diagram of a diesel locomotive model.

It is convenient to compose differential equations of oscillations of rail vehicles using the general equation of system dynamics [1]:

$$Q_l^{\alpha} + Q_l^{I} = 0; \quad l = 1,2,\ldots,K \qquad (1)$$

Preprints (www.preprints.org) | NOT PEER-REVIEWED | Posted: 7 September 2023 doi:10.20944/preprints202309.0483.v1

where Q_l^a - is the generalized force from active forces; Q_l^I - is the generalized force of inertia; K - is the number of degrees of freedom of the system.

It is convenient to calculate the generalized inertial forces using the Lagrange operator, which in the problem of small oscillations is written as:

$$Q_l^I = -\frac{d}{dt}\left(\frac{\partial T}{\partial \dot{q}_l}\right) \quad (2)$$

where $T = T(\dot{q}_l)$ - kinetic energy of the system, depending only on generalized velocities.

The generalized forces from active forces can be found through the possible power of these forces according to the formula:

$$Q_l^a = -\frac{N_{la}^*}{\dot{q}_l}; \quad (l = 1,2,...,K) \quad (3)$$

where the possible power of all given forces $(i = 1,2,...,n)$ corresponding to the generalized speed $\dot{q}_l \succ 0$ through which the possible speeds υ_i^* are expressed at each *i* -th point of application of the force is equal to:

$$N_{la}^* = \sum_i^n \vec{F}_i^a \cdot \upsilon_i^* \cdot (\dot{q}_i^*) \quad (4)$$

After substituting the values of the generalized inertial forces and the generalized active forces in (4) defined in the assumptions that $q_l^2 \le q_l$ a system of linear differential equations of small oscillations is obtained relative to the position of a stable rectilinear uniform motion of the vehicle, in which the gravity forces of individual bodies and external active forces are balanced by static values bond reactions [30]. The values of the generalized coordinates in this position are equal to zero. In translational motion, inertial forces act on the body, and in rotational motion, moments of inertia forces act on the body [2]. Consequently, the equations of motion of the body in Cartesian coordinates will take the following form:

$$\left.\begin{aligned} m\ddot{x} + \sum_{i=1}^n P_{xi} + \sum_{j=1}^k Rxj = 0 \\ m\ddot{y} + \sum_{i=1}^n P_{yi} + \sum_{j=1}^k Ryj = 0 \\ m\ddot{z} + \sum_{i=1}^n P_{zi} + \sum_{j=1}^k Rzj = 0 \\ J_x\ddot{\theta} + \sum_{i=1}^n M_{xPi} + \sum_{j=1}^k M_{xRj} = 0 \\ J_y\ddot{\theta} + \sum_{i=1}^n M_{yPi} + \sum_{j=1}^k M_{yRj} = 0 \\ J_z\ddot{\theta} + \sum_{i=1}^n M_{zPi} + \sum_{j=1}^k M_{zRj} = 0 \end{aligned}\right\} \quad (5)$$

where P_{xi}, P_{yi}, P_{zi} - is the force projections with number *i* on the *x*, *y*, *z* axes, respectively; R_{xi}, R_{yi}, R_{zi} - is the projections of reactions of elastic (or elastoviscous) elements with number *j* on the *x*, *y*, *z* axes, respectively; M_{xPi}, M_{yPi}, M_{zPi} - is the moments of forces *Pi* about axes *x*, *y*, *z*; M_{xRi}, M_{yRi}, M_{zRi} - is the moments of force R_j about axes x, y, z; J_x, J_y, J_z - is the moments of inertia of a rigid body about the axes x, y, z; $\ddot{x}$, $\ddot{y}$, $\ddot{z}$ - is the acceleration of the body along the axes x, y, z; $\ddot{\theta}$, $\ddot{\varphi}$, $\ddot{\psi}$ - is the angular accelerations of the body during its rotation around the axes x, y, z.

In Equations (5), the summation over *i* and *j* is performed algebraically, taking into account the sign of the force and the moment. To determine the sign of the force and moment, it is convenient to use the following rule: if the direction of the force or moment coincides with the direction of the forces

Preprints (www.preprints.org) | NOT PEER-REVIEWED | Posted: 7 September 2023 doi:10.20944/preprints202309.0483.v1

of inertia or the moment of the forces of inertia, then when summed they are taken with a "plus", if not, then with a "minus".

The forces of inertia, according to Newton's second law, are equal to the mass times the acceleration, and are directed in the direction opposite to the acceleration [1]. In our example, due to the arbitrary choice of the positive direction of coordinates, the positive acceleration is directed to the right, and the inertial force $m\ddot{x}$ - is the directed to the left. The same can be said about the direction of inertial forces $m\ddot{y}, m\ddot{z}$ and moments of inertia forces $J_x\ddot{\theta}$, $J_y\ddot{\varphi}$, $J_z\ddot{\psi}$.

Reactions R_j on the design scheme are directed as if they acted with a positive deformation of elastic or elastic-viscous elements. For positive deformation, you can take either tension or compression at your discretion [5]. In the diagram, the reactions are directed as if the named elements are experiencing compressive deformations.

Equations (5) are differential equations for the equilibrium of a body as it moves in a space defined by six coordinates. External forces $P = P(t)$ are, as a rule, functions of time t, and reactions R - are functions of time, coordinates and their derivatives, i.e.$R = R(t, x, y, z, \theta, \varphi, \psi, \dot{x}, \dot{y}, \dot{z}, \dot{\theta}, \dot{\varphi}, \dot{\psi})$.

These equations are written for any small period of time during which it can be assumed that the inertia forces, external forces P_i and reactions R_j, are constants. To determine the trajectory of a body in a given space under the action of external forces, it is necessary to find the functions $x = x(t), y = y(t), z = z(t), \theta = \theta(t), \varphi = \varphi(t), \psi = \psi(t)$, which, under given initial conditions, would turn the system of differential equations into an identity [3,4]. Along with the d'Alembert-Lagrange equations written in the Cartesian coordinate system, another form of notation is often used in mechanics - in the so-called generalized coordinate system. In this case, the variational equations of analytical mechanics are called the Lagrange equations of the second kind [11].

The body and bogie of a diesel locomotive are solid bodies with two degrees of freedom and connected by elastic and dissipative bonds. Wheel pairs move without separation from the rails. Perturbations from the right and left rails will be taken the same, which allows us to consider plane oscillations [6]. This formulation of the problem is quite sufficient to consider the main dynamic processes in the system [7–9].

Model six degrees of freedom. To study oscillations in the vertical longitudinal plane, we will compose a system of six second-order differential equations describing oscillations in the vertical longitudinal plane. After the transformation, we obtain Equations (6)–(8).

Body oscillation equations:

$$M_k \cdot \ddot{z}_k + b_k(2\dot{z}_k - \dot{z}_1 - \dot{z}_2) + c_k(2z_k - z_1 - z_2) = 0$$

$$J_k \cdot \ddot{\varphi}_k + z_k b_k(2a_k\dot{\varphi}_k - \dot{z}_1 + \dot{z}_2) + a_k c_k(2a_k\varphi_k - z_1 + z_2) = 0 \quad (6)$$

The oscillation equations of the first bogie:

$$M_T\ddot{z}_1 - b_k(\dot{z}_k - \dot{z}_1 + a_k\varphi_k) - c_k(z_k - z_1 + a_k\varphi_k) + 2b_T\dot{z}_1 + 2c_T = b_T(\dot{\eta}_1 + \dot{\eta}_2) + c_T(\eta_1 + \eta_2)$$

$$J_T \cdot \ddot{\varphi}_1 + 2b_T a_T^2\dot{\varphi}_1 + 2c_T a_T^2\varphi_1 = a_T[b_T(\dot{\eta}_1 - \dot{\eta}_2) + c_T(\eta_1 - \eta_2)] \quad (7)$$

Equations of vibrations of the second cart:

$$M_T\ddot{z}_1 - b_k(\dot{z}_k - \dot{z}_2 + a_k\varphi_k) - c_k(z_k - z_2 + a_k\varphi_k) + 2b_T\dot{z}_1 + 2c_T = b_T(\dot{\eta}_3 + \dot{\eta}_4) + c_T(\eta_3 + \eta_4)$$

$$J_T \cdot \ddot{\varphi}_2 + 2b_T a_T^2\dot{\varphi}_2 + 2c_T a_T^2\varphi_2 = a_T[b_T(\dot{\eta}_3 - \dot{\eta}_4) + c_T(\eta_3 - \eta_4)] \quad (8)$$

The equations of bogie oscillations Equations (6) and (7) on the right side contain expressions describing the side of the track [10].

The roughness of the path is an external perturbation of our system. The perturbation is fed to the inputs of the model with a displacement - the transport delay τ, determined by the geometric dimensions and the speed of movement:

$$\eta_i = \eta(t - \tau_i) \quad (9)$$

Preprints (www.preprints.org) | NOT PEER-REVIEWED | Posted: 7 September 2023 doi:10.20944/preprints202309.0483.v1

The choice of the type of perturbing action from the path - the roughness of the path depends on the formulation of the problem and the accuracy required for the mathematical model [16].

To analyze dynamic loads, it is necessary to obtain the acceleration values of the moving parts of the vehicle. Numerical integration subroutines used in the Mathcad package do not allow you to directly display the values of which derivatives [22]. To do this, we use the derived equations (4). Substituting in them the parameters of the crew and the obtained values of the variables of the model, we obtain expressions for acceleration in the center of the body and in the driver's cab:

$$\ddot{z}_k = \frac{1}{M_k}\left[b_k\left(-2\dot{z}_k + \dot{z}_1 + \dot{z}_2\right) + c_k\left(-2z_k + z_1 + z_2\right)\right]$$

$$\ddot{\varphi}_k = a_k / J_k\left[b_k\left(\dot{z}_1 - \dot{z}_2 - 2a_k\dot{\varphi}_k\right) + c_k\left(z_1 - z_2 - 2a_k\varphi_k\right)\right]$$

$$\ddot{z}_M = \ddot{z}_k + \left(a_k + a_T\right)\ddot{\varphi}_k \quad (10)$$

To determine the relative displacements in the hydraulic vibration dampers of the second tier, we use the following relations:

$$\ddot{z}_{01} = z_k + a_k \cdot \varphi_k - z_1$$

$$\ddot{z}_{02} = z_k - a_k \cdot \varphi_k - z_2 \quad (11)$$

To solve the resulting system of differential equations by numerical methods on a computer, it is necessary to bring the resulting equations in the Cauchy form [24]. To do this, we solve with respect to the second derivatives, and then we make a change of variables.

Initial data:

m_1:=20; j_1:=37; c_1:=6100; a_1:=1,85; b_1:=20;

m_2:=72; j_2:=493; c_2:=1500; a_2:=6.85; b_2:=100;

n_0:=0.005; w:=$2\pi\frac{v}{l}$.

$$H(z,t) = \begin{pmatrix} \frac{\left(b_1\left(\dot{\eta}_1 + \dot{\eta}_2 - 2\right) + c_1\left(\eta_1 + \eta_2 - 2z_1\right) + b_2\left(\dot{z}_k - \dot{z}_1 + \dot{\varphi}_k a_2\right) + c_2\left(z_k - z_1 + \varphi_k a_2\right)\right)}{M_T} \\ \frac{\left(b_1\left(\dot{\eta}_3 + \dot{\eta}_4 - 2\dot{z}_2\right) + c_1\left(\eta_3 + \eta_4 - 2z_2\right) + b_2\left(\dot{z}_k - \dot{z}_2 + \dot{\varphi}_k a_2\right) + c_2\left(z_k - z_2 + \varphi_k a_2\right)\right)}{M_T} \\ \frac{\left[b_2\left(\dot{z}_1 + \dot{z}_2 - 2\dot{z}_k\right) + c_2\left(z_1 + z_2 - 2z_k\right)\right]}{M_k} \\ \frac{a_1\left[b_1\left(\dot{\eta}_1 - \dot{\eta}_2 - 2\dot{\varphi}_2 a_1\right) + c_1\left(\eta_1 - \eta_2 - 2\varphi_1 a_1\right)\right]}{J_T} \\ \frac{a_1\left[b_1\left(\dot{\eta}_3 - \dot{\eta}_4\right)2\dot{\varphi}_2 a_1 + c_1\left(\eta_3 - \eta_4\right) - 2\varphi_2 a_1\right]}{J_T} \\ \frac{a_2\left[b_2\left(\dot{z}_1 - \dot{z}_2 - 2\dot{\varphi}_k a_2\right) + c_2\left(z_1 - z_2 - 2\varphi_k 8a_2\right)\right]}{J_k} \end{pmatrix}$$

7. Results and Discussion

To display the results, new variables (vectors T, Z1, Z2, V1, V2), are introduced, which are assigned the value of the columns of the solution results matrix.

The results are presented in graphical form:

- speed of vertical oscillations depending on time (Figures 25–27);

Preprints (www.preprints.org) | NOT PEER-REVIEWED | Posted: 7 September 2023 doi:10.20944/preprints202309.0483.v1

- movement over time (Figures 28–30).

Figure 25 shows the graphs of the speed of movement of the body and bogies when moving along a short unevenness (L=30 mm) with different speeds [15]. As can be seen in the figure, the first bogie at a speed of ϑ=40 km/h reaches a high oscillation amplitude of 0.05 m, and at a speed of ϑ=120 km/h the oscillation amplitude of 0.07 m. Figure 26 shows the graphs of the speed of movement of the body and bogies when moving along a short unevenness (L=100 mm) at different speeds. As can be seen in the figure, with an uneven path with a length of 100 mm and a speed of ϑ=40 km/h, the oscillation amplitude reaches 0.017 m, and at a speed of ϑ=120 km/h it reaches 0.023 m.

Figure 27 shows the graphs of the speed of movement of the body and bogies when moving along a long unevenness (L=1500 mm) at different speeds [24]. As can be seen in the figure, at a low speed ϑ=40 km/h and a long roughness of the track, the locomotive bogie reaches 0.0007 m amplitude, and at the maximum speed ϑ=120 km/h, the oscillations of the locomotive bogie reaches 0.001 m.

Based on the graphs obtained in Figures 25–27, we can conclude that with an increase in speed from 40 km/h to 120 km/h, the bogie oscillation amplitude changes (increases), which has a bad effect on the dynamics of the locomotive. On short bumps with the highest speed, the dynamics of the locomotive worsens [26].

As can be seen in Figure 28 for a short roughness (L=30 mm), the oscillation height reaches 5 mm. With an increase in speed, the frequency of amplitude oscillations increases, thereby deteriorating the smoothness of the movement of the locomotive.

In Figure 29, the height of the amplitude also reaches 5 mm, and the oscillation frequency decreases by 2 times with a decrease in the speed of movement [27–30].

In Figure 30, at speeds ϑ=40 km/h and ϑ=120 km/h, the height of the amplitude reaches 5 mm, and the oscillation frequency increases 3 times with increasing speed.

Based on the graphs obtained in Figures 28-30, it can be concluded that with a long roughness of the track, the amplitude of oscillations decreases significantly and the smoothness of the locomotive movement increases, which does not affect the dynamics of the locomotive.

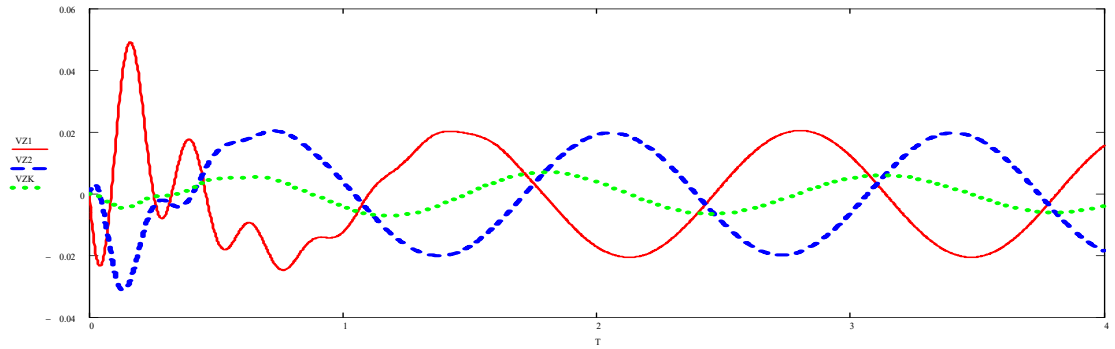

(**a**)

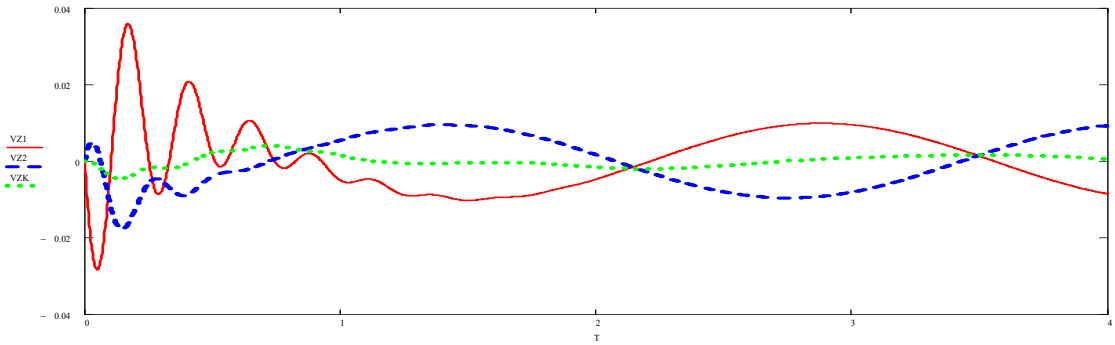

(**b**)

Preprints (www.preprints.org) | NOT PEER-REVIEWED | Posted: 7 September 2023 doi:10.20944/preprints202309.0483.v1

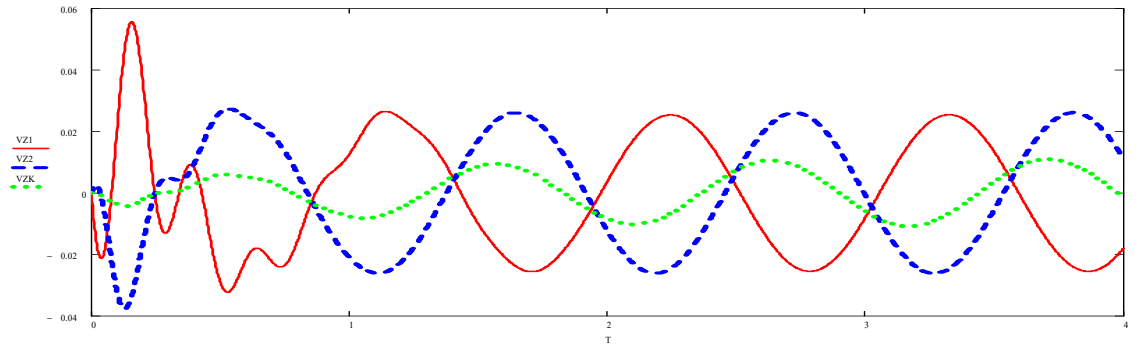

(**c**)

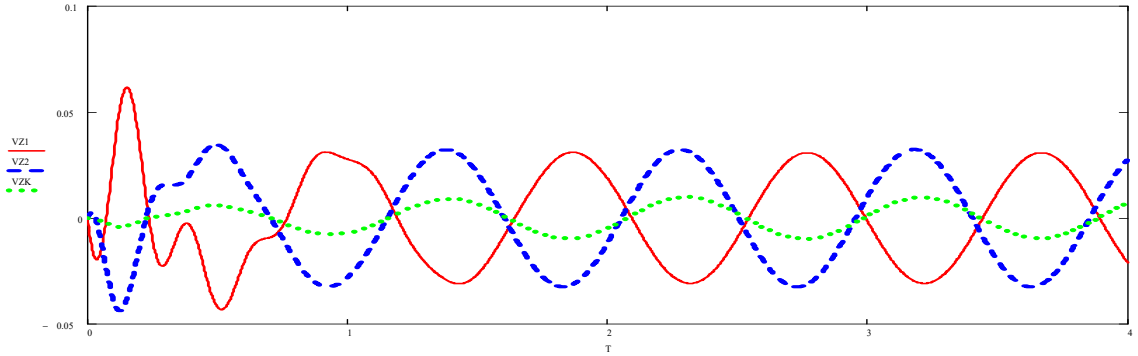

(**d**)

Figure 25. Graph of the speed of movement of the body and bogies when moving along a short unevenness (L=30 mm) with different speeds: a) ϑ=40 km/h; b) ϑ=80 km/h; c) ϑ=100 km/h; d) ϑ=120 km/h.

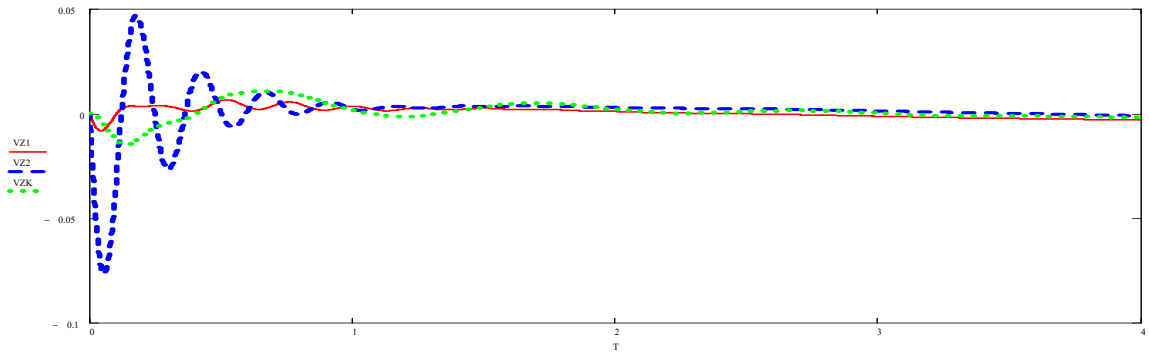

(**a**)

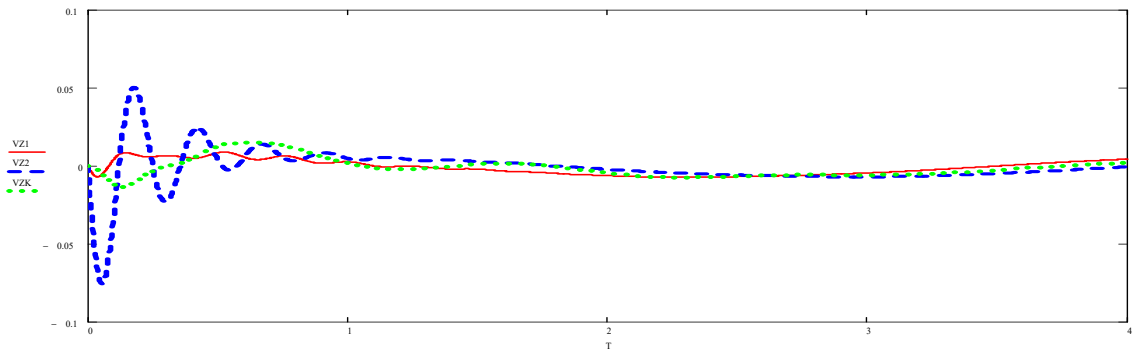

(**b**)

Preprints (www.preprints.org) | NOT PEER-REVIEWED | Posted: 7 September 2023 doi:10.20944/preprints202309.0483.v1

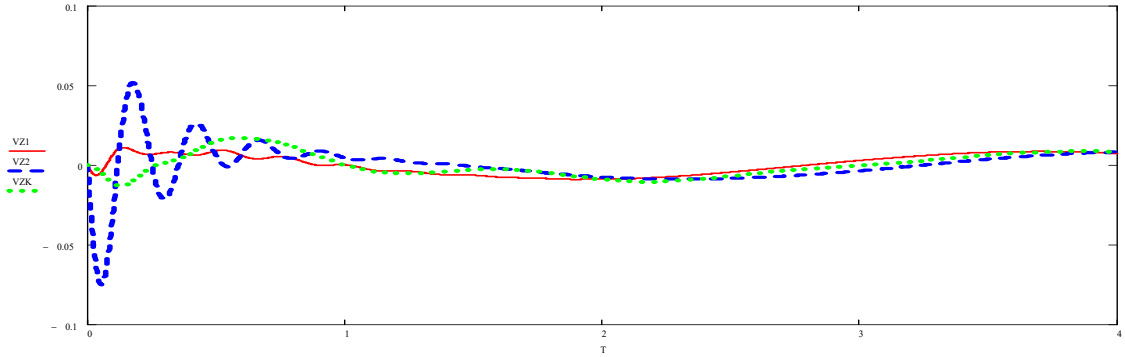

(**c**)

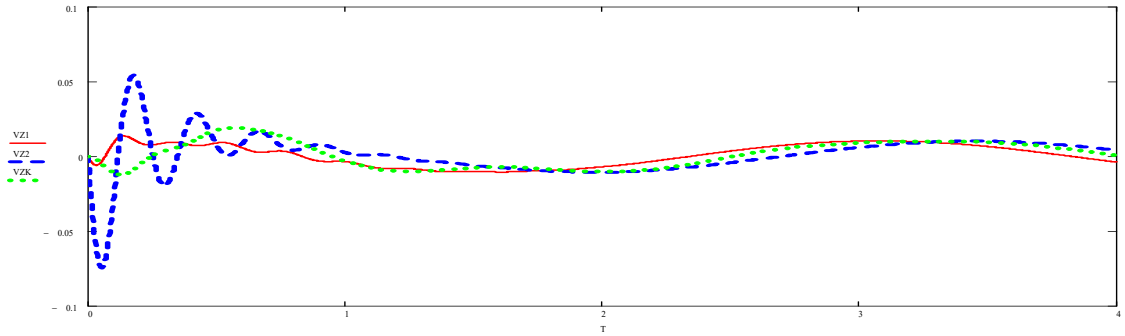

(**d**)

Figure 26. Graph of the speed of movement of the body and bogies when moving along a short unevenness (L=100 mm) with different speeds: a) ϑ=40 km/h; b) ϑ=80 km/h; c) ϑ=100 km/h; d) ϑ=120 km/h.

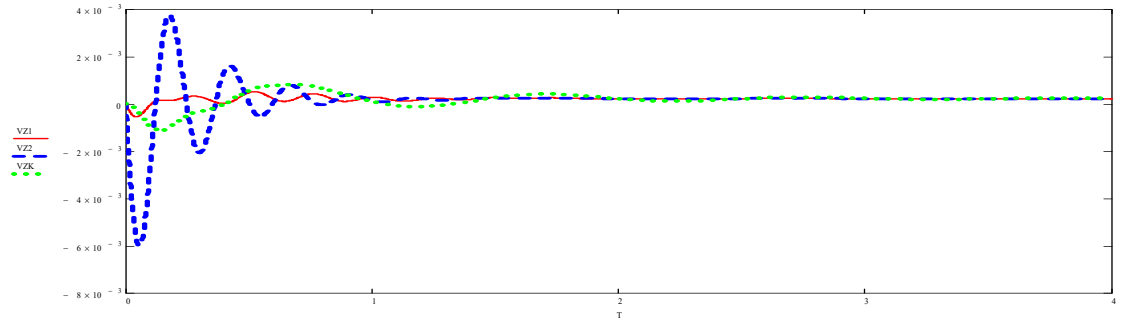

(**a**)

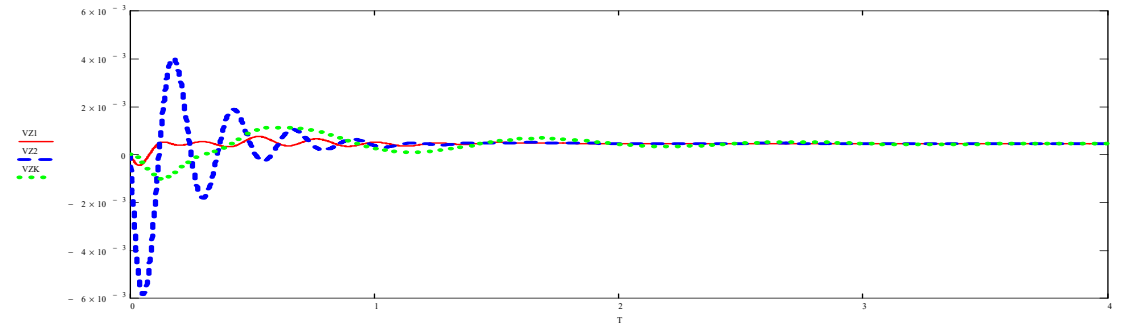

(**b**)

Preprints (www.preprints.org) | NOT PEER-REVIEWED | Posted: 7 September 2023 doi:10.20944/preprints202309.0483.v1

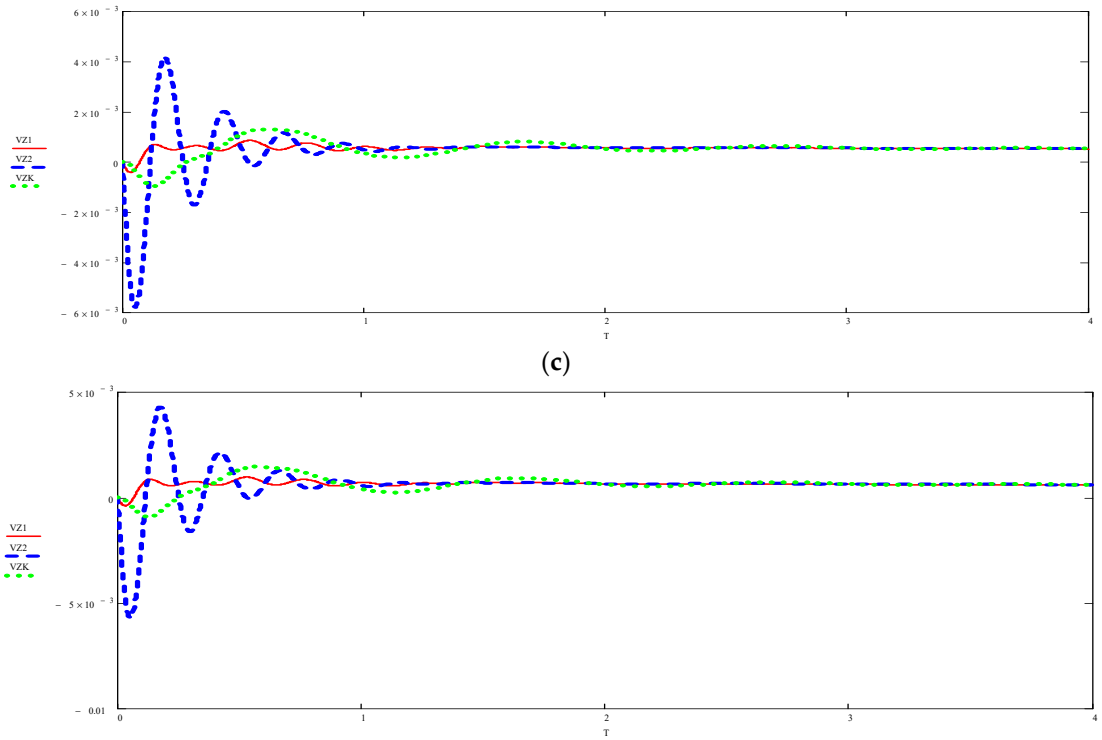

(**c**)

(**d**)

Figure 27. Graph of the speed of movement of the body and bogies when moving along a long unevenness (L=1500 mm) with different speeds: a) ϑ=40 km/h; b) ϑ=80 km/h; c) ϑ=100 km/h; d) ϑ=120 km/h.

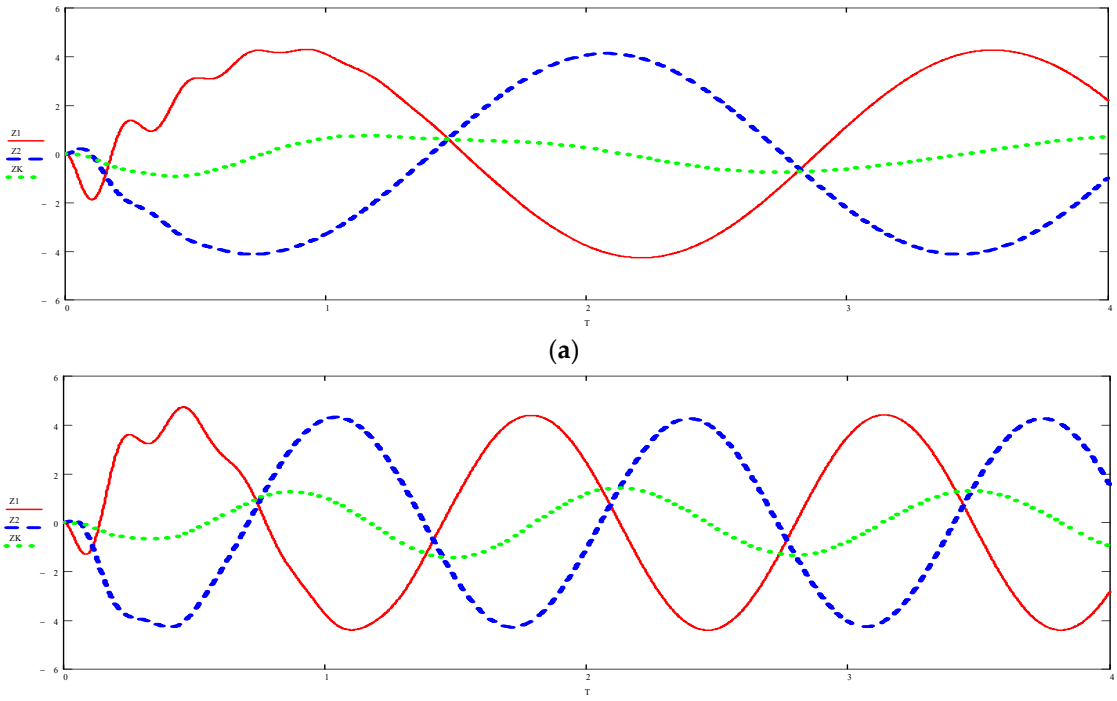

(**a**)

(**b**)

Preprints (www.preprints.org) | NOT PEER-REVIEWED | Posted: 7 September 2023 doi:10.20944/preprints202309.0483.v1

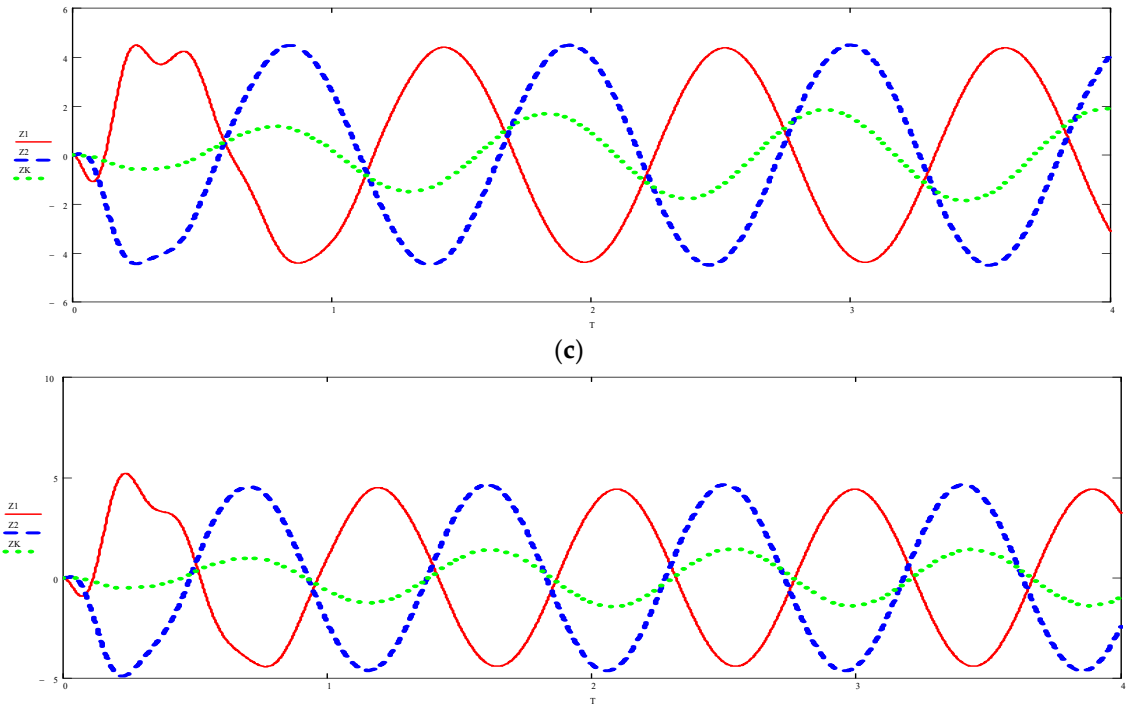

(**c**)

(**d**)

Figure 28. Graph of the movement of the body and bogies when moving along a short unevenness (L=30 mm) with different speeds: a) ϑ=40 km/h; b) ϑ=80 km/h; c) ϑ=100 km/h; d) ϑ=120 km/h.

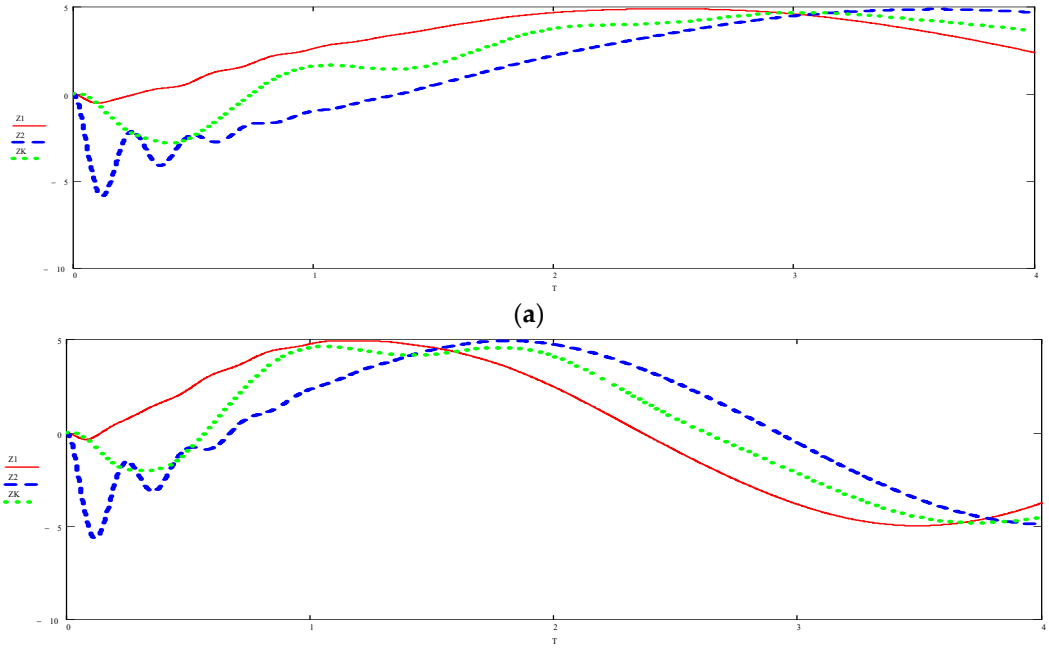

(**a**)

(**b**)

Preprints (www.preprints.org) | NOT PEER-REVIEWED | Posted: 7 September 2023 doi:10.20944/preprints202309.0483.v1

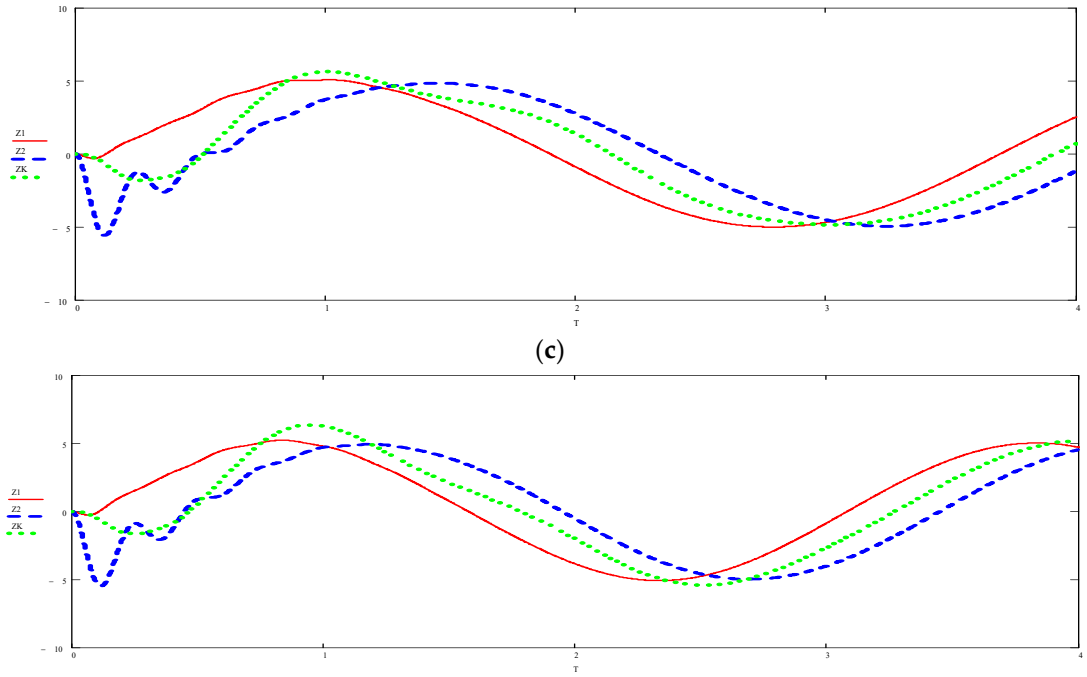

(**c**)

(**d**)

Figure 29. Graph of the movement of the body and bogies when moving along a short unevenness (L=100 mm) with different speeds: a) ϑ=40 km/h; b) ϑ=80 km/h; c) ϑ=100 km/h; d) ϑ=120 km/h.

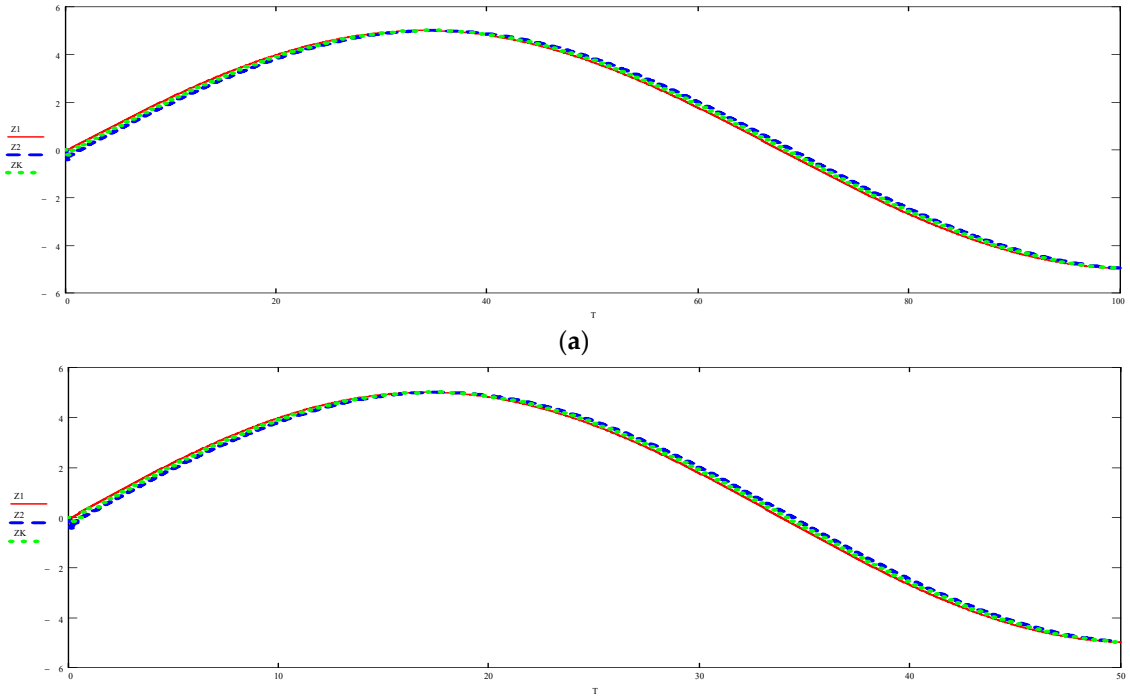

(**a**)

(**b**)

Preprints (www.preprints.org) | NOT PEER-REVIEWED | Posted: 7 September 2023 doi:10.20944/preprints202309.0483.v1

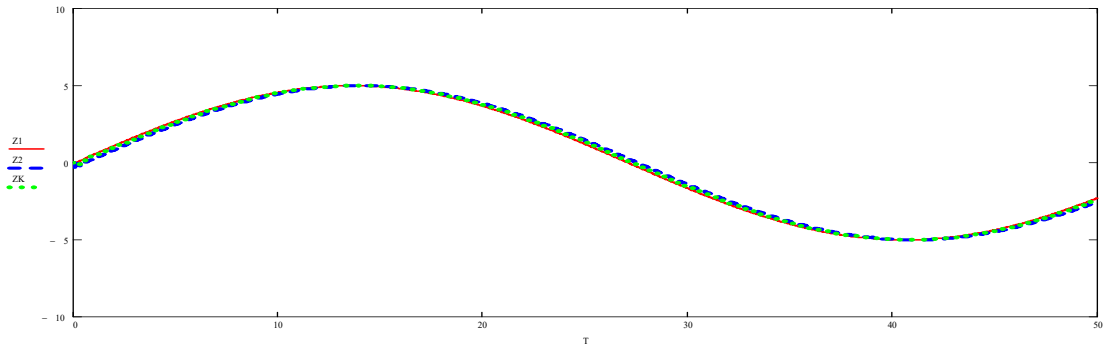

(**c**)

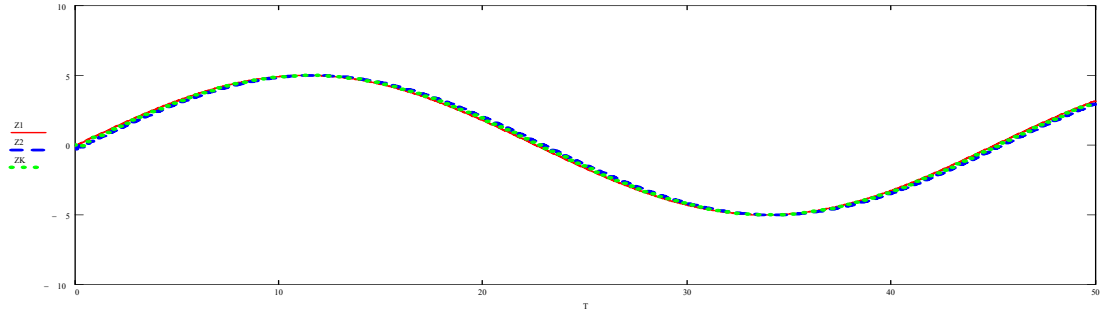

(**d**)

Figure 30. Graph of the movement of the body and bogies when moving along the length of the unevenness (L=1500 mm) with different speeds: a) ϑ=40 km/h; b) ϑ=80 km/h; c) ϑ=100 km/h; d) ϑ=120 km/h.

8. Conclusions

The performed studies allow us to draw the following main conclusions:

- experimentally obtained values of the vertical dynamics coefficients of the first and second stages of the spring suspension of the tested diesel locomotive CKD6E-2108 did not exceed the permissible limits, and the maximum values for the vertical dynamics coefficients were 0.11 for the first stage and 0.25 for the second stage. In this case, it should be noted that the obtained limit value of 0.25 of the vertical dynamics coefficient of the second stage was recorded when moving at a speed of 90 km/h, that is, 12.5% higher than the design speed [18];
- the experimentally obtained maximum value of the ratio of frame forces to the static load from the wheelset on the rails was 0.08;
- the obtained minimum value of the stability factor against derailment of the wheel on the straight section of the track is much higher than the standard value;
- thus, the speed of movement along straight sections in accordance with the Norms of permissible movement speeds according to the assessment of dynamic indicators may be limited by the declared design speed of the type of rolling stock under study [20];
- experimentally obtained dynamic performance of the investigated diesel locomotive CKD6E-2108 (the ratio of frame forces to the static load from the wheelset on the rails, the coefficients of vertical dynamics of the first and second stages of suspension and the stability factor against derailment of the wheel from the rail, registered on the track section in a curve with a radius of 400 m) meet current requirements;
- the design scheme and the equation of vertical oscillations have been developed.
- Using the MathCAD application system:

- an analysis was carried out according to the schedules of movements of the bogies and the body of the locomotive when moving along irregularities of different lengths at different speeds;
- with an increase in speed from 40 km/h to 120 km/h, the amplitude of the bogie oscillation changes (increases), which has a bad effect on the dynamics of the locomotive. On short bumps with the highest speed, the dynamics of the locomotive worsens [3];
- with a long roughness of the track, the amplitude of oscillations is much reduced and the smoothness of the movement of the locomotive increases, which does not affect the dynamics of the locomotive.

Author Contributions: Conceptualisation, J.M.; methodology, J.M. and A.Z.; software, J.M.; validation, A.Z. and J.M.; formal analysis, A.Z. and J.M.; investigation, A.Z. and J.M.; resources, S.I. and S.Y.; data curation, A.Z. and J.M.; writing—original draft preparation, A.Z.; writing—review and editing, A.Z. and J.M.; visualisation, J.M.; supervision, J.M. All authors have read and agreed to the published version of the manuscript.

Funding: This research received no external funding.

Institutional Review Board Statement: The study did not require ethical approval.

Informed Consent Statement: Not applicable.

Data Availability Statement: All data products generated in this study (velocity models, the performed studies) are available from the authors upon request.

Acknowledgments This work was carried out in the research laboratory of the Institute of Civil Engineering of the Academy of Logistics and Transport, for which the authors are grateful.

Conflicts of Interest: The authors confirm that they have no conflict of interest with respect to the work described in this manuscript.

References

1. Zhu T., Xiao S., Lei, C., Wang, X., Zhang, J., Yang, B., Yang, G., Li, Y. Rail vehicle crashworthiness based on collision energy management: an overview. International Journal of Rail Transportation. 2020, 9. 1-31.
2. Liu, P. & Wang, K. & Zhang, D. Influence of Traction and Braking Operation on Wheel-Rail Dynamic Interaction for Heavy Haul Locomotive. Zhongguo Tiedao Kexue/China Railway Science. 2017, 38. 96-104.
3. Zakeri, J.A., Xia, H. Sensitivity analysis of track parameters on train-track dynamic interaction. J Mech Sci Technol 2008, 22, 1299-1304.
4. Musayev J., Abilkaiyr Zh., Kaiym T., Alpeisov A., Alimbetov A., Zhauyt A. The interaction of the freight car and way taking into account deformation of assembled rails and sleepers. Vibroengineering PROCEDIA, 2016, 8, 269-274.
5. Musayev J., Solonenko V., Mahmetova N., Kvashnin M., Zhauyt A., Buzauova T. Modeling of dynamic characteristics of freight car with optimized parameters of wedge-type shock absorber. Journal of Vibroengineering, 2017, 19, 2, 1197-1213, 16901.
6. Wei, D.; Wei, X.; Jia, L. Automatic Defect Description of Railway Track Line Image Based on Dense Captioning. Sensors 2022, 22, 6419.
7. Biži´c, M.B.; Petrovi´c, D.Z.; Tomi´c, M.C.; Djinovi´c, Z.V. Development of method for experimental determination of wheel–rail contact forces and contact point position by using instrumented wheelset. Meas. Sci. Technol. 2017, 28, 075902.
8. Dumitriu, M.; Fologea, D.; Cruceanu, I.C. Effects analysis of vertical track irregularities on bogie vibration—Method based on bogie modelling and wheelsets accelerations measurement. IOP Conf. Ser. Mater. Sci. Eng. 2021, 1018, 012001.
9. Gao, T.; Cong, J.; Wang, P.; Liu, J.; Wang, Y.; He, Q. Vertical track irregularity analysis of high-speed railways on simply-supported beam bridges based on the virtual track inspection method. Proc. Inst. Mech. Eng. Part F J. Rail Rapid Transit 2020, 235, 328–338.
10. Li, H.; Yang, W.G.; Liu, P.; Wang, M. Prediction method and experimental verification of vibration response caused by underground high-speed railways. J. Low Freq. Noise Vib. Act. Control. 2022, 42, 452–469.
11. Olivier, B.; Verlinden, O.; Kouroussis, G. Comparison of X–T and X–X co-simulation techniques applied on railway dynamics. Multibody Syst. Dyn. 2022, 55, 39–56.

12. Bondarenko, I.; Keršys, R.; Neduzha, L. Analysis of Problem Related to Experimental Data Processing in the Study of the Rolling Stock Influence on the Track. In Proceedings of the 26th International Conference Transport Means, Kaunas, Lithuania, 5–7 October 2022; pp. 663–668.
13. Doi, H.; Hondo, T.; Nishiyama, Y.; Kuniyuki, S.; Tanaka, T. Stationary Test Method for Evaluating Wheel Unloading of Railway Vehicle on Twisted Track Simulated with Spacers between Wheel and Rail. Proc. Transp. Logist. Conf. 2020, 29, 3801.
14. Wang, H.; Berkers, J.; Hurk, N.V.D.; Layegh, N.F. Study of loaded versus unloaded measurements in railway track inspection. Measurement 2020, 169, 108556.
15. De Souza, E.F.; Bittencourt, T.N.; Ribeiro, D.; Carvalho, H. Feasibility of Applying Mel-Frequency Cepstral Coefficients in a Drive-by Damage Detection Methodology for High-Speed Railway Bridges. Sustainability 2022, 14, 13290.
16. DSTU 7571:2014; Railway Rolling Stock Permissible Exposure Norms to the Railway Track Width 1520 mm. Minekonomrozvitku: Kyiv, Ukraine, 2015.
17. Spiroiu, M.A.; Nicolescu, M. On the estimation of the reliability probabilistic model of railway wheelset. IOP Conf. Ser. Mater. Sci. Eng. 2019, 682, 012001.
18. Wang K., Huang C., Zhai W., Liu P., Wang S. Progress on wheel-rail dynamic performance of railway curve negotiation. Journal of Traffic and Transportation Engineering (English Edition). 1, 3, 2014, 209-220.
19. Ahmed K. W., Sankar S. Steady-state curving performance of railway freight truck with damper-coupled wbeelsets Vehicle System Dynamics, 26, 6, 1988, 295-315.
20. Cherkashin Y. M., Pogorelov D. Y., Simonov V. A. Influence of rolling stock and track parameters on train traffic safety. Vestnik VNIIZhT, 2, 2010, 11-20.
21. Chi M.R., Wang K.W., Fu M.H., et al. Study on curving performance for bogie with magnetic fluid coupled wheel-sets. Journal of the China Railway Society, 24, 4, 2002, 28-33.
22. Dukkipati R.V., Swamy S.N. Lateral stability and steady state curving performance of unconvertional rail truck. Mechanism and Machine Theory, 36, 5, 2001, 577-587.
23. Gialieonaido E. D., Braghin F., Biuni S. The influence of track modeling options on the simulation of rail vehicle dynamics. Journal of Sound and Vibration, 331, 19, 2012, 4246-4258.
24. Huang Y. H., Li F., Fu M. H. Research on curving performance of a bogie with independently rotating wheels. China Railway Science, 22, 6, 2001, 7-11.
25. Kurzeck B. Combined friction induced oscillations of wheelset and track during the curving of metres and their influence on corrugation. Wear, 271, 1/2, 2011, 299-310.
26. Lee S.Y., Cheng Y.C. Influences of the vertical and the roll motions of frames on the hunting stability of trucks moving on curved tracks. Journal of Sound and Vibration, 294, 3, 2006, 441-453.
27. Lu Z.G., Zhao H.X. Curve performance study and parameter design of flexible coupled single-wheelset running gears. China Railway Science, 25, 6, 2004, 32-37.
28. Ni P.T., Wang K.W., Chen J., et al. Influence of anti-hunting damper on critical velocity and high-speed curve negotiating performance of the vehicle with MRF coupled wheelsets. Journal of the China Railway Society, 29, 3, 2007, 34-39.
29. Ren Z.S., Sun S.G. Study on the influence of parameters to the dynamics of light rail vehicles with independently rotating wheel. Electric Locomotive and Mass Transit Vehicles, 26, 4, 2003, 22-24.
30. Bondarenko I., Lukoševičius V., Keršys R., Neduzha L. Investigation of Dynamic Processes of Rolling Stock–Track Interaction: Experimental Realization. Sustainability 2023, 15, 6, 5356.